A host-directed adjuvant resuscitates and sensitizes intracellular bacterial persisters to antibiotics

Kuan-Yi Lu[1], Xiangbo Yang[2], Matthew J.G. Eldridge[3], Nikki J. Wagner[1], Brian Hardy[2], Matthew Axtman[2], Sarah E. Rowe[1], Xiaodong Wang[2], Vance G. Fowler Jr[4], Sophie Helaine[3], Kenneth H. Pearce[2] and Brian P. Conlon[1,5,*]

[1]Department of Microbiology and Immunology, University of North Carolina at Chapel Hill, Chapel Hill, North Carolina, USA

[2]Center for Integrative Chemical Biology and Drug Discovery, Division of Chemical Biology and Medicinal Chemistry, University of North Carolina at Chapel Hill, Chapel Hill, North Carolina, USA

[3]Department of Microbiology, Harvard Medical School, Boston, Massachusetts, USA

[4]Division of Infectious Diseases, Duke University School of Medicine, Durham, North Carolina, USA

[5]Marsico Lung Institute, University of North Carolina at Chapel Hill, Chapel Hill, North Carolina, USA

*corresponding author: brian_conlon@med.unc.edu

Keywords: Antibiotic tolerance, MRSA, Intracellular persister, Adjuvant screen, Bacterial metabolism activation

Abstract

There are two major problems in the field of antimicrobial chemotherapy–antibiotic resistance and antibiotic tolerance. In the case of antibiotic tolerance, antibiotics fail to kill the bacteria as their phenotypic state affords them protection from the bactericidal activity of the antibiotic. Antibiotic tolerance can affect an entire bacterial population, or a subset of cells known as persister cells. Interaction with the host induces the formation of persister cells in numerous pathogens, with reactive oxygen and nitrogen species production being heavily implicated in the collapse of bacterial energy levels and entrance into an antibiotic tolerant state. Here, we developed a high-throughput screen to identify energy modulators for intracellular *Staphylococcus aureus*. The identified compound, **KL1**, increases intracellular bacterial energy and sensitizes the persister population to antibiotics, without causing cytotoxicity or bacterial outgrowth. We demonstrate that **KL1** exhibits adjuvant activity in a murine model of *S. aureus* bacteremia and intracellular infection of *Salmonella Typhimurium*. Transcriptomic analysis and further studies on its mechanism of action reveal that **KL1** modulates host immune response genes and suppresses the production of reactive species in host macrophages, alleviating one of the major stressors that induce antibiotic tolerance. Our findings highlight the potential to target intracellular persister cells by stimulating their metabolism and encourage larger efforts to address antibiotic tolerance at the host–pathogen interface, particularly within the intracellular milieu.

Introduction

Antibiotic tolerance has been frequently connected with poor treatment outcomes in the clinic (1-3). Unlike antibiotic resistance, which permits bacterial growth in the presence of

47 drugs, antibiotic tolerance allows bacteria to withstand multiple antibiotics for prolonged
48 periods (4, 5). This phenomenon is best illustrated by clinical observations in which
49 bacterial isolates that fail to respond to treatment in patients remain susceptible to the
50 prescribed antibiotics by standard minimum inhibitory concentration (MIC) testing (6, 7).
51 The extended survival of tolerant bacteria further predisposes them to evolve antibiotic
52 resistance over time, underscoring the critical need to address antibiotic tolerance (8, 9).
53
54 A principal characteristic of tolerant bacteria is their lower energy level and metabolic
55 activities, rendering a non-growing state which prevents them from being targeted by
56 antibiotics that are directed at growth-centered processes (3, 10-14). Antibiotic tolerance
57 can be induced by the infection environment and the activities of innate immune cells.
58 The intracellular environment in macrophages has been strongly associated with the
59 induction of metabolic indolence and antibiotic tolerance (15-19). Importantly, host-
60 produced reactive oxygen and nitrogen species are responsible for the induction of
61 antibiotic tolerance in a wide range of bacterial species, including *Staphylococcus aureus*,
62 *Mycobacterium tuberculosis*, *Yersinia pseudotuberculosis* and *Salmonella Typhimurium*
63 (15, 16, 18-24). Additional intracellular stressors, such as phagosome acidification and
64 nutrient deprivation, can also contribute to antibiotic tolerance (18). When conditions
65 become favorable, the intracellular bacterial persisters can resume growth, leading to
66 relapsing infections. Therefore, developing innovative strategies to target intracellular
67 bacterial persisters is essential for achieving complete eradication.
68
69 To address this difficult-to-eradicate intracellular reservoir, we established a high-
70 throughput screening platform to identify potential energy modulators, aiming to sensitize

these bacteria to antibiotics. Here, we targeted *S. aureus* as this versatile facultative intracellular pathogen is capable of surviving within various cell types (25-29) and frequently causes treatment failure and recurrent infections due to antibiotic tolerance, despite appropriate use of antibiotics (7, 30). Among the >4,700 drug-like compounds profiled, we identified that the lead compound **KL1** can resuscitate intracellular *S. aureus* and enhance antibiotic efficacy across multiple clinical isolates and laboratory strains, including methicillin-resistant *S. aureus* (MRSA). We confirm that treatment with **KL1** alone does not induce bacterial outgrowth and shows no detectable cytotoxicity in mammalian cells. Additionally, **KL1** exhibits adjuvant activity in a murine model of *S. aureus* bacteremia and intracellular infection of *Salmonella Typhimurium* within macrophages. Using transcriptomic, chemical and biochemical approaches, we discover that, rather than directly targeting the bacteria, **KL1** consistently reduces the levels of reactive oxygen and/or nitrogen species, likely through targeting the upstream regulator EHMT2/G9a. Together, we demonstrate the potential to pharmacologically sensitize intracellular bacteria to antibiotics by altering the host environment. Our energy modulator screening platform provides a pathway to uncover host-directed therapies that synergize with antibiotics and aid in the clearance of intracellular persisters.

Results

Intracellular environment is an important niche driving antibiotic tolerant *S. aureus*

Antibiotic tolerance measured in test tubes is often poorly correlated with clinical outcomes in patients, highlighting the importance of probing bacterial drug responses within the context of host–pathogen interactions (6). Multiple lines of evidence suggest that host intracellular environment serves as a privileged site of infection that antagonizes

95 antimicrobial agents for obligate and facultative intracellular bacterial pathogens,
96 including *S. aureus* (15, 17, 31-33). This phenomenon can be illustrated by testing clinical
97 isolates with varying persister frequencies in tube assays with cell-based models. We
98 found that although two *S. aureus* isolates displayed a dramatic 500-fold difference in
99 persister formation in tubes, both produced similar high-level antibiotic tolerance following
100 internalization by bone marrow-derived macrophages (BMDMs) (**Figure 1A** and **B**). Both
101 isolates produced more tolerant bacteria inside the macrophages (46–78% of the
102 intracellular bacterial population) compared to their planktonic cultures (0.03–15% of the
103 extracellular bacteria) (**Figure 1A** and **B**). These isolates had the same minimum
104 inhibitory concentrations (MICs) for rifampicin (6 to 8 ± 4 ng/mL) and other antibiotics
105 used (Supplementary table 2). This data indicates that the host interaction plays a
106 dominant role in promoting antibiotic tolerance.
107
108 As a versatile pathogen, *S. aureus* can adapt to multiple intracellular niches and colonize
109 a wide range of mammalian cells. To facilitate tracking intracellular persister cells in vivo,
110 we constructed inducible *S. aureus* fluorescent reporter strains and first demonstrated the
111 feasibility of using these reporter strains to probe intracellular *S. aureus*. We showed that
112 viable bacteria inside macrophages can be visualized using confocal microscopy and 3D
113 rendering following induction with anhydrotetracycline (aTc) (**Figure 1C** and Movie S1–
114 3). To explore whether *S. aureus* survives antibiotic treatment inside mammalian cells,
115 C57BL/6J mice were infected with the reporter strains via tail vein injections (i.v.) and
116 treated with 10 mg/kg rifampicin via the intraperitoneal (i.p.) route at 1 day post-infection
117 (dpi). Rifampicin was chosen as this drug is one of the few antibiotics that can easily
118 penetrate mammalian cells (15). The kidney cells were then extracted at 2 dpi, followed

119 by aTc treatment to induce GFP expression. The induction was performed in the presence
120 of gentamicin to exclude the extracellular bacteria. Using ImageStream analysis, we
121 observed live cells harboring GFP-expressing *S. aureus* that survived rifampicin
122 treatment (**Figure 1D**). Thus, the intracellular environment not only provides a physical
123 barrier against antimicrobial agents but also promotes antibiotic tolerance during the
124 infection. These findings reiterate the need to devise a strategy for eradicating
125 intracellular persister cells, which is particularly crucial given the limited antibiotic options
126 available against intracellular bacteria.
127

128 **A high-throughput screen for energy modulators identifies a compound that**
129 **sensitizes intracellular *S. aureus* to antibiotics**

130 Professional phagocytes, including macrophages, facilitate the clearance of bacteria
131 during bloodstream infections. However, *S. aureus* can survive this hostile environment
132 after engulfment, by adopting a less metabolically active lifestyle (25). This metabolic
133 indolence at a lower energy state favors antibiotic tolerance and persister cell formation
134 as most antibiotics are directed at growth-centered processes. To address this, we
135 developed a high-throughput platform to screen compounds that resuscitate intracellular
136 *S. aureus*, with the goal of sensitizing the intracellular population to antibiotics (**Figure**
137 **2A**). Here, we utilized a bioluminescent methicillin-resistant *S. aureus* (MRSA) strain
138 JE2–lux to probe the energy state of the intracellular bacteria (34). To assess its feasibility,
139 RAW 264.7 macrophages were infected with JE2–lux, followed by antibiotic treatment. As
140 shown in **Figure 2B**, rifampicin reduced the bioluminescent signal in the infected cells,
141 while vancomycin, which does not penetrate the mammalian plasma membrane, had no
142 effect on the intracellular *S. aureus* activity. Next, we incorporated a cell viability assay

143 into the workflow to monitor drugs' cytotoxicity. We verified that the readout reflected the
144 number of live mammalian cells without being interfered by the presence of bacteria
145 (**Figure 2C**). We then evaluated the dynamic range of the assay by measuring
146 bioluminescent signals as a function of rifampicin concentrations. The dose response
147 analysis indicated that a concentration of 2 ng/mL rifampicin resulted in a 50% reduction
148 in the intracellular bacterial activity without compromising the host cell viability (**Figure**
149 **2D**). This EC_{50} value (2 ng/mL) aligned with the rifampicin MIC (6 ng/mL) for the strain
150 JE2–lux, indicating the utility of this platform (Supplementary table 2). In comparison,
151 vancomycin did not affect the bioluminescent signal of intracellular *S. aureus* across
152 different concentrations (**Figure 2E**).
153
154 To identify energy modulators of intracellular *S. aureus* as antibiotic adjuvants,
155 macrophages infected with JE2–lux were harvested from media containing gentamicin to
156 eliminate extracellular bacteria, and then dispensed into 384-well plates with various
157 compounds (**Figure 2A**). Automatic compound dispensing was performed using a high-
158 throughput mosquito LV liquid dispenser. The bioluminescent signals and host cell
159 viability were measured immediately following a 4-hour incubation. A total of >4,700
160 compounds that share structural similarity to kinase inhibitors and comply with the
161 Lipinski's rule of five were screened (Supplementary figure 1). From this kinase-targeted
162 library, 77 compounds significantly reduced the bioluminescent signal to a level lower than
163 that of the rifampicin-treated control (three standard deviations (SD) below the control).
164 This signal reduction may indicate a decreased bacterial burden or a lower energy state
165 of the intracellular bacteria. In this screen, we did not observe any changes in persister
166 frequencies among 32 of the 77 compounds (42%) that exhibited the lowest signals.

167 Intriguingly, we identified 45 compounds that increased the bioluminescent signal by more
168 than 1.5-fold, with no detectable cytotoxicity (**Figure 3A**). We found that the top candidate
169 hit **KL1** (PubChem CID: 2881454) consistently increased the bioluminescent signal of
170 intracellular *S. aureus* (Supplementary figure 2A). This elevated signal was not a result of
171 gentamicin-killed extracellular bacteria, the host macrophages, or the compound itself
172 (Supplementary figure 2). Importantly, co-administration of **KL1** sensitized intracellular
173 MRSA to antibiotics that penetrate the mammalian plasma membrane, including
174 rifampicin and moxifloxacin, by up to 10-fold (**Figure 3B**). Treatment with **KL1** alone did
175 not induce any bacterial outgrowth, underscoring its ability to elevate the energy state of
176 intracellular *S. aureus*. The other 44 compounds did not exhibit the same adjuvant activity
177 at 10 μM, suggesting the minimum energy threshold for sensitization. To ensure its
178 reliability, we repeated the experiments using **KL1** purchased from two independent
179 suppliers and one synthesized in-house. In all cases, **KL1** increased intracellular *S.*
180 *aureus* activity and enhanced the efficacy of rifampicin in killing the intracellular bacteria
181 (Supplementary figure 3). This enhanced killing was observed across multiple laboratory
182 strains and clinical isolates, and it was proportional to **KL1**'s concentration (**Figure 3C–D**
183 and Supplementary figure 4). Furthermore, **KL1** retained its ability to synergize with
184 rifampicin even when the intracellular bacteria were pretreated with the antibiotic,
185 suggesting that low-energy persisters may be resuscitated and sensitized to antibiotic
186 treatment (**Figure 3E**). Together, we demonstrated the feasibility of pharmaceutically
187 sensitizing the intracellular *S. aureus* persisters to antibiotics and confirmed that
188 screening these sensitizers using our newly established semi-automated high-throughput
189 platform is viable.
190

191 **Compound KL1 exhibits adjuvant activity in a mouse model for *S. aureus* sepsis**
192 **and a cell-based *Salmonella* infection model**
193 Next, we evaluated the in vivo efficacy of **KL1** using our *S. aureus* bacteremia model (15).
194 Briefly, C57BL/6J mice were intravenously injected with *S. aureus* to induce a systemic
195 infection. At 6 hours post-infection (hpi), mice were administered 10 mg/kg rifampicin once
196 daily (q.d.), either alone or in combination with 100 mg/kg **KL1** twice daily (b.i.d.), via
197 intraperitoneal injections (**Figure 4A**). After a 48-hour treatment regimen, the livers and
198 spleens were harvested, and the tissue homogenates were plated to determine the
199 number of bacteria that survived the antibiotic treatment. Our data showed that combined
200 administration of **KL1** and rifampicin further reduced the bacterial burden in both the liver
201 and spleen, compared to rifampicin alone (**Figure 4B** and **C**). This animal experiment was
202 replicated on separate days using both male and female mice from different litters, which
203 each group consisting of 6–8 mice, to ensure reproducibility.
204
205 Since **KL1** may or may not directly target the bacteria and may instead modulate host–
206 pathogen interactions, we explored the possibility that **KL1** might also affect other
207 intracellular bacteria. Here, we opted to investigate the gram-negative bacterium
208 *Salmonella typhimurium* because it also survives within macrophages and forms
209 antibiotic-tolerant persister cells (18). Strikingly, **KL1** exhibited adjuvant activity when
210 combined with ciprofloxacin and enhanced the killing of *Salmonella typhimurium* in
211 macrophages (**Figure 4D**). This data suggests that **KL1** may serve as a potential broad-
212 acting antibiotic adjuvant against intracellular bacteria.
213
214 **KL1 does not directly act on *S. aureus***

215 Since the **KL1**-mediated synergy was likely energy-dependent, we utilized a mutant
216 MRSA strain lacking all four glucose transporters (ΔG4) to test if the bacterial central
217 metabolism was crucial for **KL1**'s activity (35). We found that the adjuvant activity of **KL1**
218 against intracellular *S. aureus* was substantially attenuated in the absence of functional
219 glucose uptake (Supplementary figure 5). This finding aligned with the hypothesis that
220 **KL1** enhanced antibiotic efficacy by modulating the energy state of intracellular bacteria
221 and suggested that glucose utilization was essential for sensitization of the tolerant cells.
222
223 To deconvolute **KL1**'s mechanism of action, we interrogated whether **KL1** impacted
224 extracellular *S. aureus* in planktonic cultures. We began by testing **KL1**'s activity in
225 actively growing *S. aureus* at the mid-exponential phase (high energy state). In this case,
226 no increase in energy was detected with 10 μM **KL1**, despite observing a moderate
227 increase at the higher concentration of 40 μM (Supplementary figure 6A). Treatment with
228 **KL1** at the higher concentration did not alter bacterial growth, nor did it affect persister
229 frequency following rifampicin treatment (Supplementary figure 6B). Similarly, **KL1** did not
230 affect the energy state or growth pattern of non-growing, stationary-phase bacteria (low
231 energy state) in the presence or absence of antibiotics (Supplementary figure 6C and D).
232
233 We subsequently employed Seahorse analysis to investigate whether **KL1** altered the
234 metabolic activity of extracellular *S. aureus*. This analysis measures real-time changes in
235 cellular metabolism and has been applied to investigate bacterial respiration in *S. aureus*
236 (36). Our data clearly showed that **KL1** had no effect on the oxygen consumption rate
237 (OCR) and extracellular acidification rate (ECAR) of *S. aureus* in planktonic cultures
238 (Supplementary figure 7A and B). Additionally, we directly measured the relative ATP

239 levels in the bacteria and did not observe any changes across multiple *S. aureus* strains
240 (Supplementary figure 7C–E). Collectively, our data strongly suggested that **KL1** did not
241 directly target the bacteria but may perturb the host–pathogen interaction by altering the
242 intracellular environment.
243
244 **KL1 modulates the host cells and reduces the level of reactive species**
245 To elucidate **KL1**'s mode of action, we profiled the transcriptomic changes of *S. aureus*-
246 infected macrophages in response to the treatment using bulk RNA-sequencing. In
247 comparison with the vehicle control, **KL1** treatment resulted in the up-regulation of 24
248 genes and the down-regulation of 90 genes (**Figure 5**). The **KL1**-mediated changes were
249 enriched in inflammatory responses, cytokine production and macrophage activation.
250 However, the treatment did not appear to obliterate the host immune response, and
251 treatment with **KL1** alone did not cause bacterial outgrowth. Intriguingly, multiple host
252 genes involved in regulating reactive oxygen and nitrogen species (ROS/RNS) were
253 identified (**Figure 5B and C**). Important genes promoting ROS/RNS production, such as
254 *Thbs1*, *S100a8*, *Nos2* and *Maf*, were significantly down-regulated, while a glutathione S-
255 transferase gene *Gsta2*, involved in the cellular anti-oxidative defense was up-regulated
256 (37, 38). As such, **KL1** may alleviate the oxidative and nitrosative stress in the intracellular
257 niche, which aligns with previous findings that ROS/RNS can induce antibiotic tolerance
258 and persister cells in intracellular *S. aureus* and various bacterial species (15, 16, 18-21,
259 39).
260
261 Although the exact mechanism of **KL1** has not been determined, this compound has been
262 included in hundreds of biological screens. Among these screens, **KL1** was found to be

263 active in five bioassays targeting four different proteins (Supplementary table 3).
264 EHMT2/G9a, in particular, stood out as a potential candidate target of **KL1** given that this
265 epigenetic regulator is an intracellular protein expressed in immune cells, including
266 macrophages. Additionally, the EC_{50} values of **KL1** (25 μM) determined in the previous
267 EHMT2/G9a inhibition assay (PubChem AID: 504332) aligned with the adjuvant activity
268 of **KL1** (10–40 μM) identified in this study. Intriguingly, EHMT2/G9a plays a key role in the
269 intracellular innate immunity and modulates macrophage polarization through the
270 regulation of inflammatory genes, such as *Il6* and *Il1b* (40-44). It can also regulate NF-κB
271 and JAK/STAT signaling (43). This downstream regulation is partly reminiscent of our
272 findings in **KL1**-mediated gene expression shift (**Figure 5**). To interrogate EHMT2/G9a
273 as a potential target, we first utilized the highly selective EHMT inhibitor BIX-01294 to
274 assess whether EHMT2/G9a influences antibiotic susceptibility of intracellular *S. aureus*.
275 Surprisingly, we found that inhibition of EHMT2/G9a also elevated the energy state of
276 intracellular *S. aureus* and synergized with rifampicin in a dose-dependent manner,
277 similar to the effect observed with the identified compound **KL1** (**Figure 6A** and **B**). Given
278 the role of EHMT2/G9a in modulating inflammatory responses and our findings that **KL1**
279 alters the expression of genes involved in ROS/RNS production, we hypothesized that
280 **KL1** targets EHMT2/G9a and alleviates the production of ROS/RNS, thereby facilitating
281 the antibiotic killing of intracellular bacteria. To test this hypothesis, we employed two
282 probing methods with distinct detection mechanisms to measure reactive species.
283 Specifically, a chemiluminescent probe L-012 and a fluorescent probe fluorescein-
284 boronate (Fl-B) were applied (16, 45). Using both methods, we consistently observed that
285 **KL1** at 40 and 100 μM significantly reduced the levels of ROS/RNS in *S. aureus*-infected
286 macrophages at 4- and 8-hours post-treatment (**Figure 6C–D** and Supplementary figure

287 8A and C). Notably, treatment with the EHMT2/G9a inhibitor BIX-01294 and the
288 antioxidant control butylated hydroxyanisole (BHA) both resulted in a similar decrease in
289 ROS/RNS. Furthermore, **KL1** was able to lessen the levels of ROS/RNS in uninfected
290 macrophages, highlighting its ability to adjust the host environment (Supplementary figure
291 8B and D).
292
293 **Inactive analog of KL1 losses the ability to modulate the level of reactive species**
294 To provide further insight into the medicinal chemistry, we conducted a brief structure–
295 activity relationship study using six analogs of **KL1** and tested how different chemical
296 modifications interfered with their biological activity (**Figure 7A**). The substitution of
297 carboxamide at the alkyl terminal (KL2, KL4 and KL5) or removal of the nitrile group from
298 the dihydropyridine ring (KL6) led to moderate potency loss in sensitizing intracellular
299 bacteria to rifampicin (**Figure 7B**). The hexyl substitution on sulfur (KL3) resulted in a high
300 cytotoxicity against host macrophages, rendering a poor therapeutic index for targeting
301 intracellular bacteria. Notably, the 1,4-dihydropyridine ring oxidized analog (KL7)
302 completely lost the adjuvant activity, presumably resulted from the altered electronic
303 structure, decreased conformational flexibility or loss of hydrogen bonding capacity
304 (**Figure 7B**). Importantly, this inactive analog KL7 also lost the ability to reduce host-
305 derived reactive species in both infected and uninfected macrophages (**Figure 7C** and
306 Supplementary figure 9). Altogether, these results strongly support the hypothesis that
307 **KL1** enhances antibiotic killing of intracellular bacteria by reducing oxidative and/or
308 nitrosative stress in the intracellular milieu, presumably by targeting the epigenetic
309 regulator EHMT2/G9a (**Figure 8**).
310

311 ## Discussion

312 The ability of bacterial populations or sub-populations of persister cells to survive high
313 concentrations of bactericidal antibiotics for extended periods, despite lacking resistance
314 mutations, is likely a major factor contributing to treatment failure. Approximately 20–30%
315 of patients with *S. aureus* bacteremia fail to clear the infection despite receiving
316 appropriate antibiotic therapy (46-48). The weak correlation between in vitro antimicrobial
317 susceptibility and clinical outcomes highlights the importance of considering the relevant
318 physiological context when addressing the poor antibiotic efficacy in clinical settings (6).
319

320 Devising novel strategies to target antibiotic tolerant persister cells has drawn increasing
321 attention over the years (14, 49-51). Conceptually, the eradication of persister cells can
322 be achieved either by directly targeting the persister cells or by reverting them to a
323 metabolically active state, thereby making them vulnerable to antibiotics. The intracellular
324 environment is a well-established reservoir for antibiotic tolerant persister cells (15-19).
325 In this study, we demonstrated the potential of altering the host microenvironment to
326 sensitize intracellular persisters to antibiotics and improve treatment outcomes. Although
327 different stress stimuli can lead to the formation of antibiotic tolerant persister cells, most
328 produce a metabolically indolent state that can withstand antibiotic challenge. We
329 therefore employed an ATP-dependent bioluminescent reporter to probe the energy levels
330 of intracellular bacteria as part of a phenotypic screen. When combined with a host cell
331 viability measurement and CFU determination, this platform allowed us to identify
332 molecules that activate intracellular persister cells without compromising host viability or
333 inducing expansion of the pathogen. Given that the low-energy, low-metabolic activity
334 state is central to antibiotic tolerance and persistence in multiple bacterial species, this

335 screening may be adapted for other intracellular pathogens across various host cell types
336 and will be agnostic to the mechanism responsible for the induction of antibiotic tolerance
337 (52-55).
338
339 Intriguingly, our lead compound **KL1** significantly reduced ROS/RNS production in
340 macrophages, sensitized intracellular *S. aureus* and *Salmonella* persister cells to
341 antibiotic treatment, and enhanced antibiotic efficacy in a murine infection model.
342 Transcriptomic analysis further support a mechanism associated with an altered
343 inflammatory response and reduced ROS/RNS production. These observations are in line
344 with a previous biochemical activity screen in which **KL1** inhibited the activity of
345 EHMT2/G9a that epigenetically regulates a wide range of biological processes, including
346 macrophage polarization (40-44). Consistently, inhibition of EHMT2/G9a mirrored the
347 activity of **KL1** and caused sensitization of intracellular *S. aureus*, implicating that
348 EHMT2/G9a may be the primary target of **KL1** (**Figure 8**).
349
350 Together, these findings strongly support that: 1) Targeting host pathways can render
351 intracellular persisters more susceptible to antibiotics; 2) ROS/RNS are key drivers of
352 antibiotic tolerance in vivo; 3) Inhibiting ROS/RNS production can sensitize persister cells
353 across diverse bacterial species; and 4) Sensitizing intracellular persisters leads to
354 improved antibiotic efficacy against active infections. This work underscores the potential
355 of using host-directed therapeutics, in conjunction with antibiotics, to enhance treatment
356 outcomes. Continued development of our screening platform promises identification of
357 additional host-targeted drugs that sensitize intracellular persisters to antibiotics. Ongoing
358 studies on **KL1**'s mechanism of action, along with medicinal chemistry optimization and

359 in vivo testing in combination with various antibiotics against multiple pathogens, including
360 *M. tuberculosis*, will be critical in determining the full therapeutic potential of this host-
361 directed adjuvant in eradicating deep-seated infections.
362

363 Materials and methods

364 General materials

365 Antibiotics including rifampicin (Rif), moxifloxacin hydrochloride (Mox), gentamicin sulfate
366 (Gen) were purchased from Fisher Scientific with >95% purity. Vancomycin hydrochloride
367 (Van) (>99% purity) was purchased from Alfa Aesar. Compound **KL1** was obtained from
368 multiple sources (ChemBridge Corporation, Enamine and synthesized in-house
369 (Supplementary Information)) with >90% purity to validate the fidelity of this compound.
370 Analogs KL2–6 were purchased from ChemDiv, ChemBridge Corporation and Vitas M
371 Chemical Limited (>90% purity). Analog KL7 was synthesized in-house with >90% purity
372 (Supplementary Information). The G9a inhibitor, BIX-01294 (>98% purity), was
373 purchased from MedChemExpress. RAW 264.7 macrophages were obtained from ATCC
374 (TIB-71) and distributed by the Tissue Culture Facility at the University of North Carolina
375 at Chapel Hill. RAW 264.7 cells were maintained in complete DMEM (Dulbecco's Modified
376 Eagle Medium (Gibco) supplemented with 10% (vol/vol) heat-inactivated fetal bovine
377 serum (FBS) (Avantor Seradigm, premium grade), 2 mM L-glutamine (Gibco), 1x non-
378 essential amino acids solution (Gibco) and 1 mM sodium pyruvate (Gibco)) below 18
379 passages without reaching more than 90% confluency. Bone marrow-derived
380 macrophages (BMDMs) were isolated from C57BL/6J mice (The Jackson Laboratory;
381 strain number 000664) and cultivated in complete DMEM as previously described (56).
382 Immortalized BMDMs were generated using a CRE-J2 retroviral infection method (57).

383 Briefly, C57BL/6J mouse-derived BMDMs were cultured in 50% (vol/vol) L929 fibroblast-
384 conditioned medium and infected with CRE-J2 retrovirus on day 5 and day 7. Transduced
385 cells were continuously cultured in the conditioned medium, with the concentration
386 gradually reduced to 20% conditioned medium. The immortalized BMDMs were
387 maintained in RPMI 1640 (Corning) supplemented with 2 mM L-glutamine, 1x Penicillin-
388 Streptomycin (GenClone), 10% (vol/vol) heat-inactivated FBS (R&D Systems) and 20%
389 conditioned medium.
390

391 **Bacterial strains and growth conditions**

392 *S. aureus* strains LAC (USA300), HG003, JE2 (USA300), JE2–lux (JE2*lux*ABDCE)
393 (kindly provided by Roger Plaut, Center for Biologics Evaluation and Research, Silver
394 Spring, United States) (34), ΔG4 (kindly provided by Anthony Richardson, University of
395 Pittsburgh, Pittsburgh, United States) (35) and the *S. aureus* bacteremia isolates (16)
396 were routinely cultured in tryptic soy broth (TSB) (Fisher Scientific) at 37 °C and 225 rpm
397 unless otherwise stated. The clinical isolates were obtained under an IRB exemption from
398 a preexisting collection. *Salmonella enterica serovar Typhimurium* strain 14028S was
399 cultured in LB broth (Lennox) at 37 °C with shaking.
400

401 **Minimum inhibitory concentration assay**

402 Stationary-phase bacterial cultures were diluted at 1:1,000 in Mueller–Hinton broth (MHB)
403 (Oxoid) containing serially diluted Rif (0–0.2 μg/mL), Mox (0–20 μg/mL) or Van (0–16
404 μg/mL) in 96-well assay plates (Corning) in triplicates (200 μL/well). Plates were sealed
405 with Breathe-EASIER membranes (Diversified Biotech) and incubated statically at 37 °C
406 for 24 h. The minimum inhibitory concentrations (MICs) were determined by the absence

407 of bacterial growth. Three independent assays were performed to ensure the
408 reproducibility.
409
410 **Construction of the inducible reporter strains**
411 The plasmid pALC2084 containing a tetracycline (Tet)-inducible GFP-expressing cassette
412 (58) (kindly provided by Ambrose Cheung, Dartmouth College, Hanover, United States)
413 was transformed into a *S. aureus* intermediate strain RN4220 using a Gene Pulser Xcell
414 electroporation system (Bio-Rad) as previously described (59). The plasmid was
415 subsequently purified and transformed into the recipient *S. aureus* strain HG003. Single
416 colonies were isolated and cultured in TSB containing 10 μg/mL Cam and 0–2 μM
417 anhydrotetracycline hydrochloride (aTc) (Sigma) for 2–3 h. The induction of GFP
418 expression was verified at an excitation and emission wavelength of 475 nm and 508 nm
419 using a Synergy H1 microplate reader (BioTek). To construct the mKate reporter plasmid,
420 the DNA fragment of mKate2 was amplified from pRN10 (Addgene plasmid: 84454) (60)
421 using a specific primer pair (Supplementary table 1) and Q5 High-Fidelity DNA
422 Polymerase (New England Biolabs). The PCR product was purified using a MinElute
423 Reaction Cleanup kit (Qiagen). A Tet-inducible expression vector pRMC2 (Addgene
424 plasmid: 68940) (61) and the mKate DNA fragments were subjected to KpnI-HF and
425 EcoRI-HF (New England Biolabs) enzymatic digestion and agarose gel electrophoresis.
426 The DNA fragments were gel purified using a QIAquick PCR purification kit (Qiagen) and
427 underwent ligation with T4 DNA ligase (New England Biolabs) at 16 °C for 16 h. The
428 ligation product was transformed into MAX Efficiency DH5α competent cells
429 (ThermoFisher Scientific) according to the manufacturer's instruction. Site-directed
430 mutagenesis was performed using a QuikChange kit (Agilent Technologies) and a primer

431 pair (Supplementary table 1) to incorporate an upstream ribosomal binding site. The final
432 pRMC2-mKate construct was verified by restriction digest mapping and Sanger
433 sequencing. The plasmid pRMC2-mKate was transformed into strain RN4220, followed
434 by the recipient strain HG003 as described above. The aTc-induced mKate expression
435 was confirmed by measuring at 633 nm with excitation at 588 nm using a Synergy H1
436 microplate reader.
437
438 **Antibiotic survival assays**
439 For *S. aureus* planktonic cultures, 16- to 18-h stationary cultures were diluted at 1:100 in
440 MHB and incubated at 37 °C and 225 rpm for 3 h to reach the mid-exponential phase.
441 The bacterial cultures were then treated with 10 μg/mL Rif and/or 0–40 μM **KL1** at 37 °C
442 and 225 rpm for 24 h. The bacteria were washed in one volume of sterile 1% NaCl three
443 times at 20,000 *g* for 5 min, followed by resuspending in one volume of 1% NaCl. The
444 bacterial suspensions were 10-fold serially diluted and plated on tryptic soy agar (TSA)
445 to enumerate the number of survivor *S. aureus*. The frequencies of tolerant bacteria were
446 calculated by normalizing the numbers of survivor bacteria to the numbers of input
447 bacteria (T_0).
448
449 To assess the intracellular *S. aureus* persister frequencies, RAW 264.7 macrophages or
450 BMDMs were seeded in Costar 24-well tissue culture-treated plates (Corning) (500 μL of
451 $4x10^5$ cells per well) in complete MEM (Minimum Essential Medium (Gibco)
452 supplemented with 10% (vol/vol) heat-inactivated fetal bovine serum and 2 mM L-
453 glutamine) at 37 °C and 5% CO_2 for 16 h. Macrophages were infected with *S. aureus*
454 strains at a multiplicity of infection (MOI) of 10 by centrifugation at 1,000 *g* for 2 min,

455 followed by incubation at 37 °C for 35 min. After removal of the spent medium, infected
456 cells were incubated in 500 μL complete MEM containing antibiotics (10 μg/mL Rif, 50
457 μg/mL Mox or 20 μg/mL Van) in the presence or absence of 0–40 μM **KL1** and its analogs
458 (KL2–7) or 0–10 μM BIX-01294 in the presence of 50 μg/mL Gen at 37 °C and 5% CO_2
459 for 24 h. The cells were washed three times in 1 mL PBS and lysed with 200 μL 0.5%
460 (vol/vol) Triton X-100 (Fisher Scientific) at 37 °C for 5 min, followed by the addition of 800
461 μL PBS. The released intracellular *S. aureus* were 10-fold serially diluted and plated on
462 TSA for enumeration. For the persister frequencies, the numbers of survivor bacteria were
463 normalized to the corresponding numbers of intracellular bacteria before the antibiotic
464 treatment (T_0). For comparison between different treatment groups, the intracellular *S.*
465 *aureus* loads were normalized against the untreated controls at the endpoint (24-h post-
466 treatment).
467
468 For *Salmonella* infections, immortalized BMDMs were seeded in 12-well tissue culture-
469 treated plates ($4x10^5$ cells per well) in RPMI 1640 supplemented with 2 mM L-glutamine
470 and 10% (vol/vol) heat-inactivated FBS at 37 °C and 5% CO_2 for 24 h. The stationary-
471 phase bacteria were opsonized with 8% (vol/vol) mouse serum in the RPMI 1640 medium
472 for 20 min and applied to the immortalized BMDMs at an MOI of 15 as previously
473 described (32). The plates were centrifuged at 110 *g* for 5 min and incubated at 37 °C and
474 5% CO_2 for 30 min. Cells were washed once with PBS and incubated in RPMI 1640
475 medium containing 5 μg/mL ciprofloxacin hydrochloride (MP Biomedicals) in the presence
476 of 10–80 μM **KL1** or 0.2% DMSO at 37 °C and 5% CO_2 for 24 h. The cells were washed
477 three times in 500 μL PBS and lysed with 0.2% (vol/vol) Triton X-100 at 37 °C for 10 min.
478 The extracted intracellular *Salmonella Typhimurium* were plated on LB agar to determine

479 the number of survivor bacteria. The persister frequencies were calculated by normalizing
480 the final CFUs (T_{24}) to the input CFUs (T_0).
481
482 **Live cell microscopy**
483 RAW 264.7 macrophages were seeded in a Nunc 8-well Lab-Tek chambered coverglass
484 (ThermoFisher Scientific) (500 µL of 2–3x10^5 cells per well) in complete MEM at 37 °C
485 and 5% CO_2 for 16 h. Cells were infected with the Tet-inducible GFP- or mKate-
486 expressing *S. aureus* strains at an MOI of 20 (without Rif) or 100 (with Rif) by
487 centrifugation at 1,000 *g* for 2 min and incubating at 37 °C for 35 min. Cells were washed
488 once in 500 µL complete MEM and treated with and without 10 µg/mL Rif in the presence
489 of 50 µg/mL Gen at 37 °C for 1.5 h (without Rif) and 4 h (with Rif). Rif-treated cells were
490 washed three times with 500 µL complete MEM and incubated in the medium containing
491 50 µg/mL Gen at 37 °C for 2–3 h to allow for resuscitation of the intracellular *S. aureus*
492 persisters. Infected cells were then treated with 2 µM aTc in the presence of 50 µg/mL
493 Gen at 37 °C for 3 h to induce GFP and mKate expression. Macrophages harboring GFP-
494 expressing *S. aureus* were imaged using a Leica SP8X Falcon (Leica Microsystems) with
495 the following settings: (1) a tunable white light laser (WLL2) set to 484 nm was used for
496 excitation with fluorescence detection at 495–570 nm and a detector gain of 100 V; (2) a
497 1024 X 1024 pixel scan at 16-bit with a scanning speed set to 600 was applied; (3) the
498 pixel averaging was set to 2; (4) the pinhole size was set to 1 AU; (5) single images were
499 obtained using a 63x oil-immersion objective lens (Plan-Apochromat, NA 1.4) with an 1
500 to 4-fold zoom. Macrophages infected with mKate-expressing *S. aureus* were stained with
501 100–300 nM LysoTracker Green DND-26 (ThermoFisher Scientific) at 37 °C for 30 min.
502 The dye-loaded cells were washed once and kept in 200 µL complete MEM containing 1

503 μg/mL Hoechst 33342, 50 μg/mL Gen and 2 μM aTc. The z-stack acquisition and time-
504 lapse live imaging were carried out using an Olympus FV3000RS confocal microscope
505 (Olympus Life Science) equipped with a stage-top incubator at 37 °C, 5% CO_2 and 100%
506 humidity. The microscope settings were as follows: (1) 405-nm (Hoechst 33342), 488-nm
507 (LysoTracker Green) and 594-nm (mKate) diode lasers were used for excitation with
508 highly sensitive fluorescence spectral GaAsP detectors; (2) a 516 X 516 pixel scan was
509 applied; (3) the pixel averaging was set to 10; (4) the pinhole size was set to 1 AU; (5)
510 single images were obtained using a 60x oil-immersion objective lens (Super Correction,
511 NA 1.4). All confocal images were exported as the default with no gamma correction by
512 ImageJ/FIJI (62).
513
514 **Mouse infection and isolation of kidney cells**
515 C57BL/6J mice (6- to 9-week-old) were systemically infected with the Tet-inducible GFP-
516 expressing *S. aureus* strain HG003 ($5x10^6$ CFU) via the tail vein intravenous route (15).
517 At 1 day post-infection (dpi), mice were administered with 10 mg/kg Rif in 2.5% DMSO,
518 12.5% polyethylene glycol (PEG300) (Sigma) and 85% sterile H_2O via intraperitoneal
519 injection. Infected mice received the vehicle (2.5% DMSO/12.5% PEG300) were included
520 as a control. At 2 dpi (24-h Rif treatment), dissected mouse kidneys were homogenized
521 in 5 mL cold PBS containing deoxyribonuclease I (50 U/mL, bovine pancreas)
522 (ThermoFisher Scientific) using a Stomacher 80 Biomaster (Seward, USA) at fast speed
523 for 2 min twice (63). Tissue homogenates were filtered through 70-μm strainers (VWR
524 International) and pelleted at 300 *g* for 5 min at 4 °C. After three washes in 4 mL cold PBS
525 in 5-mL polypropylene round-bottom tubes (Corning) at 300 *g* for 5 min at 4 °C, cells were
526 resuspended in cold PBS containing 1% fetal bovine serum and 50 μg/mL Gen in the

527 presence or absence of 2 μM aTc for 3 h. The cell suspensions were probed with
528 LIVE/DEAD fixable violet dead cell stain (1 μL/1 mL) (ThermoFisher Scientific) at 4 °C for
529 30 min before ImageStream analysis.
530
531 To evaluate the adjuvant activity of **KL1** in vivo, C57BL/6J mice were infected by
532 intravenous injection with $2x10^7$ CFU of *S. aureus* strain HG003. At 6 hours post-infection
533 (hpi), mice were administered with 10 mg/kg Rif, either alone or in combination with 100
534 mg/kg **KL1** in 7% DMSO, 40% PEG300 and 53% sterile H_2O via intraperitoneal injection.
535 Rif and **KL1** were administered once a day (q.d.) and every 12 h (b.i.d.), respectively, for
536 2 days. After 48 h treatment, dissected mouse organs were homogenized either by
537 repetitively rolling a serological pipette over the samples in the sample bags (liver) or by
538 bead beating using a Precellys 24 Touch (Bertin Technologies) at 5,000 rpm for 25 s twice
539 with a 5 s interval (spleen). Tissue homogenates were 10-fold serially diluted in 1% NaCl
540 and plated on TSA for the enumeration of survivor bacteria. The bacterial burden (CFU/g)
541 was calculated by normalizing the number of CFU to the tissue weight.
542
543 **ImageStream analysis**
544 Cell suspensions were loaded into an Amnis ImageStreamX Mark II (EMD Millipore) for
545 single-cell imaging and fluorescence detection. For capturing live cells harboring viable
546 GFP-expressing *S. aureus*, 405-nm and 488-nm colinear lasers were set to 40 mW and
547 70–90 mW for the live/dead cell discrimination and GFP expression, respectively. In-focus
548 single-cell images were acquired with a 60X magnification and a low-speed flow rate
549 using the INSPIRE software (EMD Millipore). The exported data were analyzed using
550 IDEAS 6.2 software (EMD Millipore).

551

552 **High-throughput screen for intracellular *S. aureus* energy modulators**

553 RAW 264.7 macrophages were seeded in 4 mL complete MEM in Costar 6-well tissue
554 culture-treated plates (Corning) ($8x10^5$ cells/well) at 37 °C and 5% CO_2 for 16 h. Cells
555 were infected with *S. aureus* strain JE2–Lux at an MOI of 100 at 37 °C for 25 min. The
556 infected macrophages were washed once with 2 mL PBS and incubated with 10 mM
557 EDTA in PBS (2 mL/well) at 37 °C for 5–10 min. After dissociation, cells were pelleted at
558 300 *g* for 6 min, resuspended in complete MEM containing 50 µg/mL Gen at a density of
559 $2.5x10^5$ cells/mL and dispensed 80 µL of the cell suspension into each well of 384-well
560 tissue culture-treated white plates and optically clear polymer bottom black plates
561 (ThermoFisher Scientific) for luminescence and fluorescence detections, respectively.
562 Uninfected macrophages were also added to column 1 and 24 of each plates as controls
563 for the luminescence background and the baseline of host cell viability. The plates were
564 preloaded with 80 nL of 10 mM compounds using a Mosquito LV multichannel pipetting
565 system (SPT Labtech, Covina). The vehicle control (0.1% DMSO) and 10 µg/mL Rif were
566 included in each experiment for comparison. After cell dispensing, the plates were
567 centrifuged at 500 *g* for 2 min and incubated in a humidified chamber at 37 °C and 5%
568 CO_2 for 4 h. The luminescence signals were measured at an 1.25-mm depth with a
569 detector gain of 250 at 37 °C using a Synergy H1 microplate reader. To monitor the cell
570 viabilities after compound treatment, 10 µL CellTiter-Fluor reagent (Promega) were added
571 to the black plates and incubated in the dark at 37 °C and 5% CO_2 for 30 min. The
572 fluorescence intensities were measured at a 7-mm depth with a detector gain of 100 at
573 37 °C. The kinase-targeted compound library containing >4,700 rule of five-compliant
574 compounds were part of the chemical collection at the Center for Integrative Chemical

575 Biology and Drug Discovery (CICBDD) at the University of North Carolina at Chapel Hill.
576 The luminescence and fluorescence signals were normalized to the corresponding
577 vehicle controls (0.1% DMSO). EC_{50} values of Van and Rif for the intracellular MRSA
578 strain JE2–Lux were determined by fitting the luminescence data to a standard dose
579 response equation (GraphPad Prism).
580
581 **Reactive species assays**
582 The reactive oxygen and nitrogen species were measured using a luminescent probe L-
583 012 (Wako Chemical Corporation) and a fluorescent dye fluorescein-boronate (Fl-B) (56).
584 For L-012 probing, RAW 264.7 macrophages were seeded in 100 μL complete MEM in
585 Falcon 96-well tissue culture-treated white plates (Corning) (3.84×10^4 cells/well) at 37 °C
586 and 5% CO_2 for 16 h. Cells were infected with *S. aureus* strain JE2 at an MOI of 10 by
587 centrifugation at 1,000 *g* for 2 min, followed by incubation at 37 °C for 40 min. Cells were
588 treated with 40–100 μM **KL1** or 1–10 μM BIX-01294 in the presence of 50 μg/mL Gen in
589 five replicates at 37 °C and 5% CO_2 for 4–8 h. After three washes with 200 μL pre-warmed
590 PBS, 100 μL of 300 μM pre-warmed Hanks' balanced salt solution (Gibco) was added to
591 each well. The luminescence signals were immediately measured with auto-gain at 37 °C
592 using a Synergy H1 microplate reader. The signals of two consecutive reads were
593 averaged to minimize the technical variability between reads. For Fl-B staining,
594 macrophages were seeded in 96-well tissue culture-treated black clear-bottom plates
595 (Corning) with the same culture condition. After treatment with 40–100 μM **KL1**, 100 μM
596 KL2, 40–100 μM the inactive analog KL7, 1–10 μM BIX-01294 or 20 μM butylated
597 hydroxyanisole (Sigma), infected cells were washed twice with 200 μL pre-warmed PBS
598 and incubated with 100 μL of 25 μM Fl-B in PBS at 37 °C for 30 min. Cells were washed

599 three times with 200 μL PBS to remove unbound dyes and maintained in 100 μL PBS.
600 The fluorescence signals were measured at 535 nm with excitation at 485 nm with a
601 detector gain of 100 and an area scan mode using a Synergy H1 microplate reader.
602
603 **ATP measurement**
604 *S. aureus* strains LAC, HG003 and JE2 were grown in TSB for 16–18 h and subcultured
605 at 1:1,000 to 1:40,000 dilution in fresh TSB containing 40 μM **KL1** or 0.1–0.5% DMSO in
606 six replicates at 37 °C for 4 h. The bacterial cultures were then aliquoted into Falcon 96-
607 well white plates (100 μL/well) and mixed with one volume of BacTiter-Glo reagent
608 (Promega), followed by incubation in the dark on a rocker with gentle shaking at room
609 temperature for 20 min. The luminescence signals were detected at a 1.25-mm depth
610 with a detector gain of 250 using a Synergy H1 microplate reader and normalized to the
611 corresponding CFUs to determine the relative ATP levels.
612
613 **Seahorse analysis**
614 The stationary-phase bacterial cultures were diluted at 1:100 in fresh TSB in triplicate and
615 incubated for 2–3 h until the OD_{600} values reached 0.3. Each culture was then diluted at
616 1:500 to 1:1,000 in TSB or Seahorse XF DMEM (Agilent Technologies) supplemented
617 with 100 mM glucose, 2 mM L-glutamine and 1 mM sodium pyruvate and dispensed into
618 a poly-D-lysine (PDL)-coated Seahorse XF HS miniplate (100 μL/well). PDL-coating was
619 performed by adding 100 μg/mL PDL in sterile H_2O to each well of the miniplate for 30
620 min. Excessive PDL was removed by two washes with H_2O, and the miniplate was air-
621 dried prior to the assays. Bacteria adherence was achieved by centrifugation at 1,400 *g*
622 for 10 min. An additional 80 μL media was carefully added to each well (180 μL final

623 volume), and the miniplate was loaded into a pre-calibrated Seahorse XF HS Mini
624 Analyzer (Agilent Technologies). A final concentration of 40 μM of **KL1** or 0.1–0.5%
625 DMSO was injected into each well, and the oxygen consumption rates (OCRs) and
626 extracellular acidification rates (ECARs) of the bacteria were monitored at 37 °C for 4–6
627 h. The data was analyzed using Seahorse Analytics (Agilent Technologies) and plotted
628 using GraphPad Prism.
629
630 **Transcriptomic analysis**
631 RAW 264.7 macrophages were seeded in 4 mL complete MEM in 6-well tissue culture-
632 treated plates ($8x10^5$ cells/well) at 37 °C and 5% CO_2 for 16 h. Cells were infected with
633 *S. aureus* strain JE2–Lux at an MOI of 20 at 37 °C for 35 min and incubated in fresh
634 media containing 100 μg/mL Gen and 40 μM **KL1** or 0.1% DMSO at 37 °C for 24 h. After
635 a PBS wash, cells were dissociated with 10 mM EDTA in PBS (2 mL/well) at 37 °C for 5
636 min, followed by three washes in 10 mL PBS at 4 °C to remove EDTA. The number of
637 viable host cells was enumerated to ensure consistent sample input ($2.4–4.2x10^6$ total
638 viable cells for both **KL1**- and DMSO-treated groups). The frozen cell pellets were
639 delivered to Azenta Life Sciences for the standard RNA-sequencing (paired-end, 30
640 million reads per sample) and data analysis. The aligned sequencing data were mapped
641 to mouse GRCm38 reference genome available on ENSEMBL using the STAR aligner
642 v.2.5.2b.
643
644 **Databases**
645 Biological test results of the identified compound **KL1** (PubChem CID: 2881454) were
646 retrieved from PubChem (https://pubchem.ncbi.nlm.nih.gov/) (64). Gene expression

647 profiles were examined using Expression Atlas (https://www.ebi.ac.uk/gxa/home) (65).
648 Biological functions and subcellular localization data were sourced from the UniProt
649 Knowledgebase (https://www.uniprot.org/) (37). Protein association networks among the
650 differentially expressed genes were analyzed using STRING (https://string-db.org/) (66).
651 Chemical structures were gene rated using ChemDraw software 21.0.0 (PerkinElmer).
652

653 **Acknowledgements**

654 This work was supported by the Burroughs Wellcome Fund (BWF) in Pathogenesis of
655 Infectious Disease (PATH award to B.P.C), the National Institutes of Health (NIH)
656 (R01AI173004 and R01AI179695 to B.P.C and R01AI167978 to S.E.R) and UNC
657 Lineberger Comprehensive Cancer Center. The content of this study is solely the
658 responsibility of the authors and does not necessarily represent the official views of the
659 funding agents. We are grateful to the UNC Neuroscience Microscopy Core and the UNC
660 Flow Cytometry Core Facility (supported in part by P30 CA016086). Part of the figures
661 was created with BioRender.com.
662

663 **Contributions**

664 K.L. and B.P.C. conceptualized the project and wrote the manuscript. K.L. performed
665 the genetic engineering, in vitro and animal experiments. K.L. and N.J.W. performed the
666 Seahorse analyses. K.L., B.H. and M.A. performed the high-throughput screen. X.Y.
667 synthesized the compounds. M.J.G.E. performed the *Salmonella* infection assays.
668 V.G.F. provided *S. aureus* clinical isolates. B.P.C. and S.E.R. provided funding for the
669 project. B.P.C., S.E.R., X.W., S.H. and K.H.P. supervised the study. All the authors
670 reviewed and edited the manuscript.

Footnotes

To whom correspondence should be addressed. Email: brian_conlon@med.unc.edu

The authors have no competing interests.

676 ## Figures

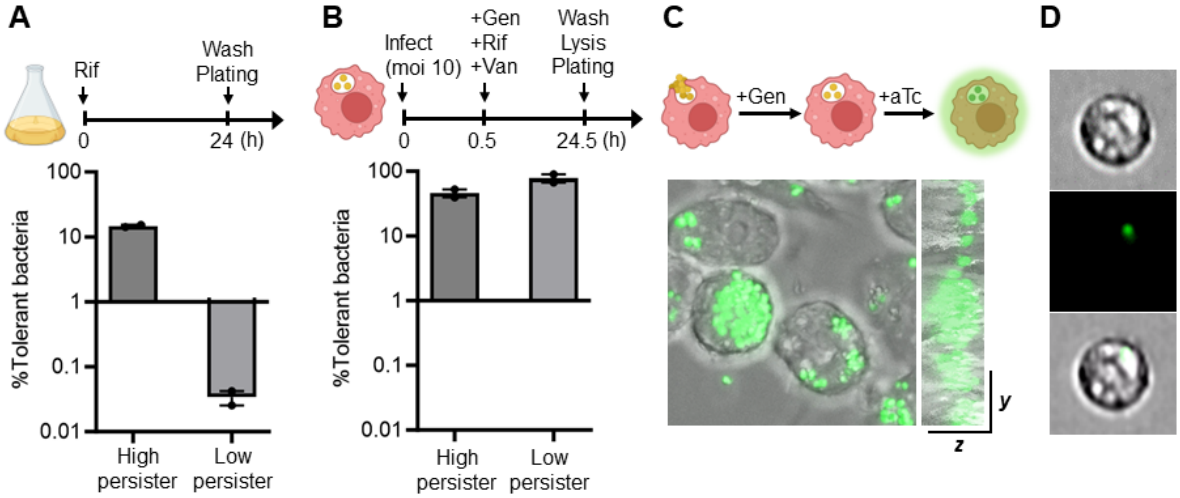

677

678 **Figure 1. Intracellular environments provide an important niche producing**
679 **antibiotic-tolerant *S. aureus* persisters.** (**A**) Clinical isolates from *S. aureus* bacteremia
680 patients exhibited variable antibiotic tolerability in planktonic cultures. Rifampicin (Rif) was
681 washed away to enumerate the numbers of survivor bacteria (CFU). (**B**) The high and low
682 persister isolates characterized in (**A**) became more tolerant and produced comparable
683 numbers of persisters in bone marrow-derived macrophages. Gentamicin (Gen) and
684 vancomycin (Van) were administered to eradicate the extracellular bacteria. The numbers
685 of survivor bacteria were normalized to the corresponding numbers of intracellular CFUs
686 before the antibiotic treatment (T_0) to calculate the persister frequencies. Representative
687 data of three independent experiments are shown (n = 3). The bars represent mean ±
688 SEM. Assay schematics are shown above plots. (**C**) Confocal z-sectioning visualized
689 viable intracellular *S. aureus*. RAW 264.7 macrophages were infected with an inducible
690 GFP reporter strain and treated with 50 μg/mL Gen to exclude extracellular *S. aureus*.
691 Live intracellular bacteria can be probed with anhydrotetracycline (aTc) induction. (**D**)
692 Intracellular persisters in mouse kidneys were detected using ImageStream analysis.

693 C57BL/6J mice were systemically infected with the inducible reporter strain via the
694 intravenous route and intraperitoneally treated with 10 mg/kg Rif at 1 day post-infection
695 (dpi) for 24 h. The kidney cells were extracted at 2 dpi and incubated with 2 μM aTc to
696 induce GFP expression. Representative images are shown.
697
698

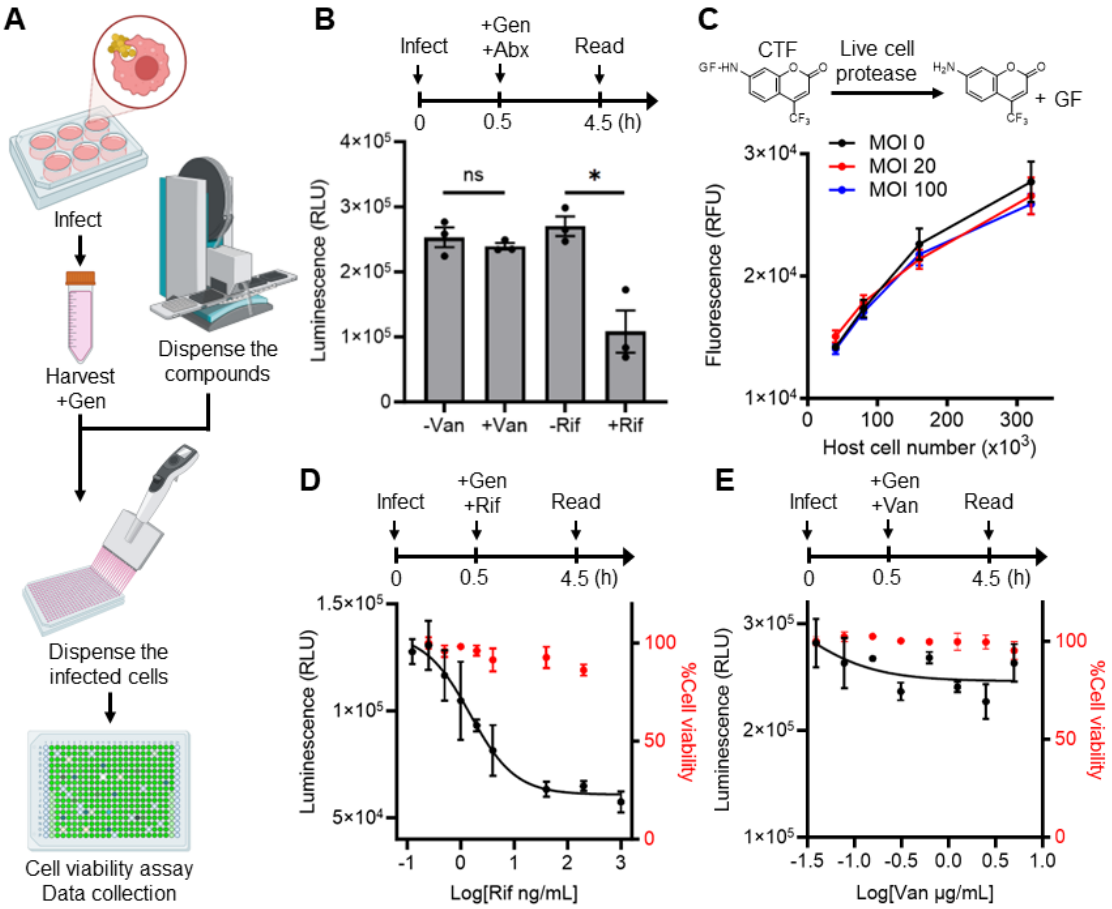

Figure 2. An established high-throughput screen allows for identifying compounds that modulate the energy state of intracellular *S. aureus*. (**A**) Schematic representation of the constructed compound screen for energy modulators of the intracellular bacteria. (**B**) The intracellular *S. aureus* activity can be probed using a bioluminescent MRSA strain JE2–lux. RAW 264.7 macrophages were infected with JE2–lux and treated with 20 µg/mL vancomycin (Van) or 10 µg/mL rifampicin (Rif) for 4 h before luminescence detection. Gentamicin (Gen; 50 µg/mL) was also added to eliminate the extracellular bacteria. Only Rif can penetrate the host plasma membrane and target the intracellular bacteria. Representative data of three biological replicates is shown (n = 3). *p<0.05; ns, not significant (unpaired t-test). The bars represent mean ± SEM. (**C**) The

710 host cell viability can be monitored using CellTiter-Fluor (CTF). The enzymatic reaction
711 reflected the number of viable RAW 264.7 cells (Pearson correlation coefficient $r > 0.97$,
712 $p < 0.05$) and was not interfered with the presence of *S. aureus*. The multiplicities of
713 infection (MOIs) of 0 (black), 20 (red) and 100 (blue) are shown (n = 3). (**D** and **E**) Dose
714 response curves for Rif (**D**) and Van (**E**) inhibition of intracellular *S. aureus* activity (black
715 circles). The host cell viability was simultaneously measured (red circles). Representative
716 data of three biological replicates is shown (n = 3). The bars represent mean ± SEM.
717 Assay schematics are shown above plots.
718
719

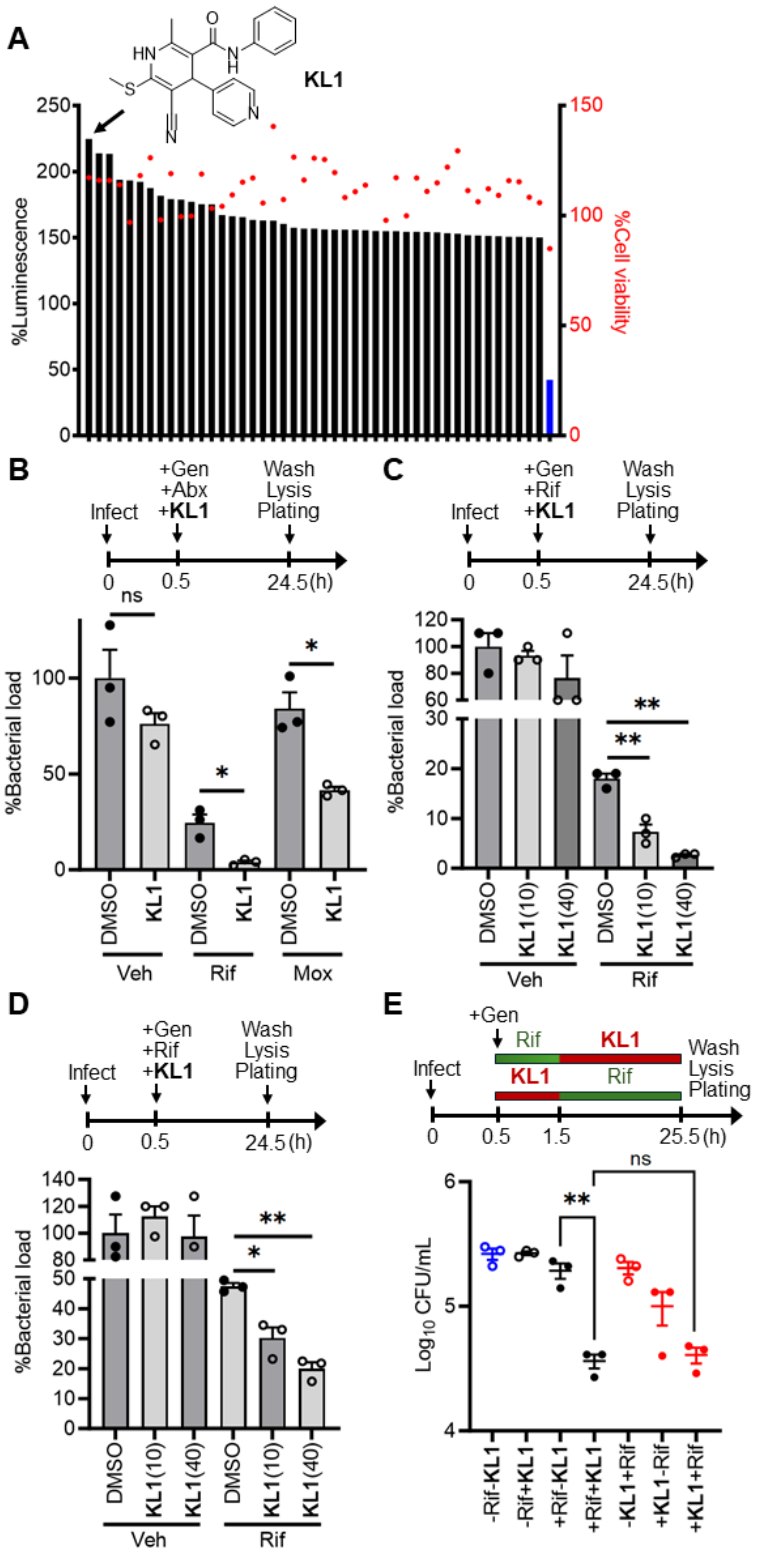

720

721 **Figure 3. Screening a kinase-targeted compound library identifies a small molecule**

722 **that sensitizes intracellular *S. aureus* to antibiotic killing.** (**A**) Forty-five compounds

723 (10 μM) exhibited >1.5-fold increase in the luminescence signal (black bars) comparing
724 to the vehicle control (0.1% DMSO). No cytotoxicity was observed in the 4-h treatment
725 window (red circles). The chemical structure of the top candidate compound **KL1** is shown.
726 The rifampicin-treated group was included as a reference (blue bar). (**B**) **KL1** (open
727 circles) facilitates rifampicin (Rif; 10 μg/mL) and moxifloxacin (Mox; 50 μg/mL) killing of
728 the intracellular MRSA. Gentamicin (Gen; 50 μg/mL) was added to eradicate the
729 extracellular bacteria. The numbers of survivor bacteria were normalized to the untreated
730 control (no antibiotics (Abx), no **KL1**, Gen-only) (n = 3). (**C** and **D**) The **KL1**-mediated
731 synergism was detected in different clinical isolates with the high persister (**C**) and low
732 persister (**D**) phenotypes characterized in Figure 1A. A dose-dependent sensitization was
733 observed with 0–40 μM **KL1** in these isolates (n = 3). (**E**) Pre-exposure to Abx does not
734 affect the sensitization by **KL1**. Infected RAW 264.7 cells were treated with either 10
735 μg/mL Rif (black circles) or 40 μM **KL1** (red circles) for 1 h, followed by the addition of
736 **KL1** and Rif, respectively. The untreated group (blue circles) was included as a negative
737 control (n = 3). Assay schematic above plot indicates the orders of the treatment regimens.
738 *p<0.05; **p<0.01; ns, not significant (unpaired t-test). The bars represent mean ± SEM.
739
740
741
742

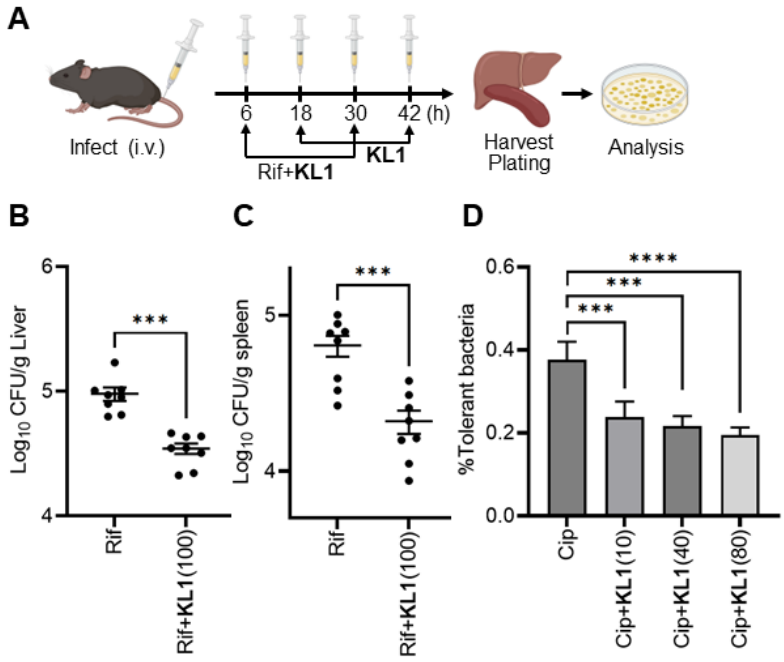

743

744 **Figure 4. The identified compound KL1 enhances antibiotic killing of *S. aureus* in a**
745 **murine bacteremia model and *Salmonella Typhimurium* in macrophages.** (**A**)
746 Schematic representation of the murine model. C57BL/6J mice were infected via
747 intravenous (i.v.) tail vein injections and intraperitoneally treated with 10 mg/kg rifampicin
748 (Rif) (q.d.) with and without 100 mg/kg **KL1** (b.i.d.) at 6 hours post-infection (hpi) for 2
749 days. The organs were harvested and homogenized to enumerate the numbers of
750 survivor bacteria (CFU). Co-administration of **KL1** and Rif reduced the bacterial burden
751 in the liver (**B**) and spleen (**C**). Representative data of two independent experiments is
752 shown (n = 8). A total of 14 mice per treatment group were examined. ***p<0.001
753 (unpaired t-test). (**D**) **KL1** facilitates ciprofloxacin (Cip; 5 μg/mL) killing of intracellular
754 *Salmonella Typhimurium*. The numbers of survivor bacteria were normalized to the input
755 CFUs (T_0) (n = 7–8). ***p<0.001; ****p<0.0001 (two-way ANOVA). The bars represent
756 mean ± SEM.

757

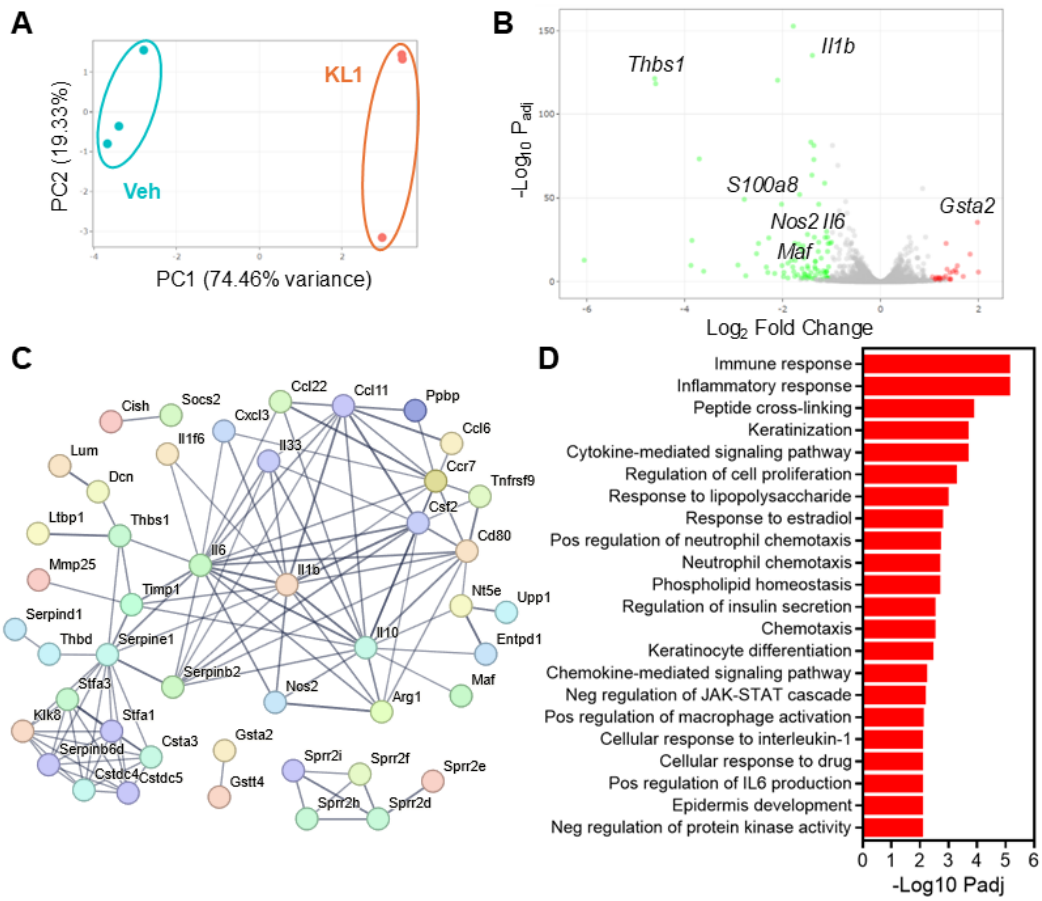

Figure 5. KL1 modulates the expression of host immune response genes regulating reactive oxygen and nitrogen species. Principle component analysis (**A**), differential expression (**B**) and String network (**C**) analysis illustrate the **KL1**-mediated transcriptional modulation in *S. aureus*-infected macrophages (n = 3). Genes associated with reactive species production are indicated. Edge thickness represents the confidence in the interactions. Interactions with high confidence (interaction score >0.7) are shown. (**D**) Gene ontology enrichment with an adjusted p-value <0.01 is shown.

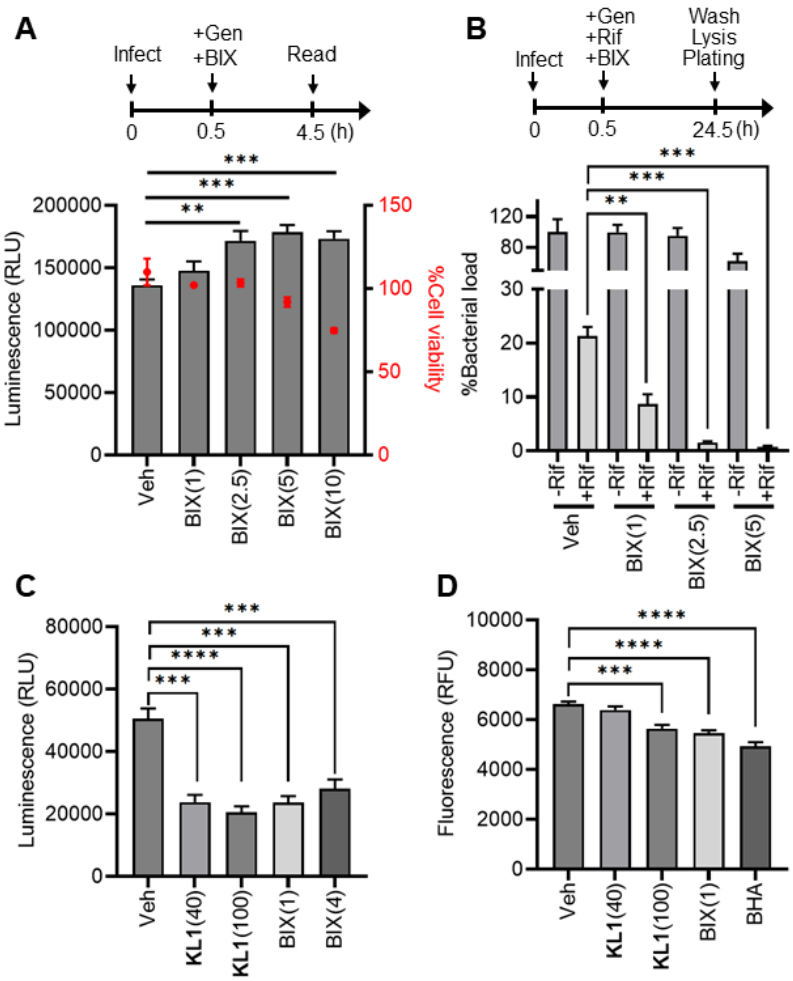

Figure 6. KL1 reduces the production of reactive species upon infection. (**A**) Inhibition of G9a/EHMT2 phenocopies the **KL1**-mediated sensitization in intracellular *S. aureus*. A selective G9a inhibitor, BIX-01294 (BIX; 2.5–10 μM), increased the bioluminescence signal (grey bars) of strain JE2–lux comparing to the vehicle control (Veh, 0.1% DMSO). The relative cytotoxicity of BIX was examined (red circles). Representative data of three independent experiments is shown (n = 5). (**B**) The G9a inhibitor increases rifampicin (Rif; 10 μg/mL) killing of the intracellular MRSA in a dose-dependent manner (1–5 μM). Gentamicin (Gen; 50 μg/mL) was added to eradicate the extracellular bacteria. The numbers of survivor bacteria were normalized to the untreated control (no Rif, no BIX, Gen-only) (n = 3). Both **KL1** (40 and 100 μM) and BIX (1 and 4

778 μM) reduced ROS production at 4 hours post-infection (hpi). A chemiluminescent probe
779 L-012 (**C**) and a fluorescent probe fluorescein-boronate (Fl-B) (**D**) were utilized to quantify
780 reactive species in infected macrophages. An antioxidant butylated hydroxyanisole (BHA;
781 20 μM) was included as a control. Representative data of three independent experiments
782 are shown (n = 5). Assay schematics are shown above plots. **$p<0.01$; ***$p<0.001$;
783 ****$p<0.0001$ (unpaired t-test). The bars represent mean ± SEM.
784
785

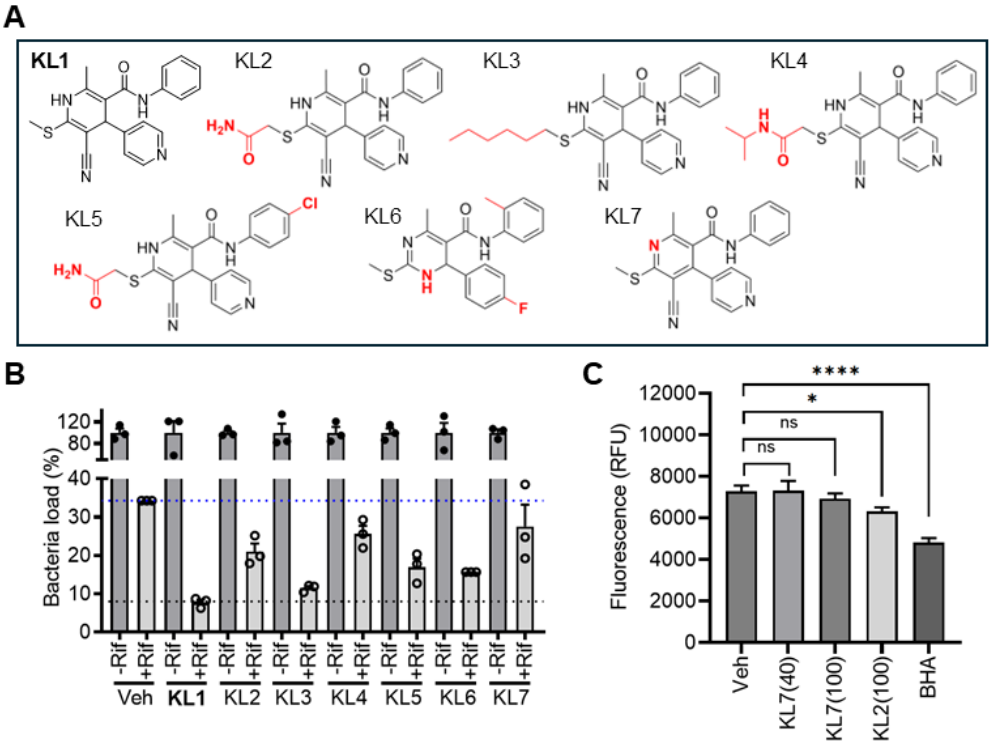

Figure 7. KL1 analogs with attenuated adjuvant activity loss the ability to regulate reactive species production. (**A**) Chemical structures of **KL1** and its analogs. Modified functional groups were indicated in red. (**B**) **KL1** analogs (40 μM) exhibited differential activities in sensitizing intracellular *S. aureus* to antibiotic killing. Infected cells were treated with (open circle) and without (solid circle) rifampicin (Rif; 10 μg/mL) and various analogs. Gentamicin (50 μg/mL) was added to eliminate the extracellular bacteria. The relative bacterial loads were normalized to the corresponding controls (-Rif). (**C**) The inactive analog KL7 (40 and 100 μM) and KL2 (100 μM) with reduced adjuvant activity showed no and minimum effect on ROS/RNS production in infected macrophages, respectively. DMSO (Veh) and an antioxidant butylated hydroxyanisole (BHA; 20 μM) were included as controls. Representative data of three biological replicates is shown (n = 3). *p<0.05; ****p<0.0001; ns, not significant (unpaired t-test). The bars represent mean ± SEM.

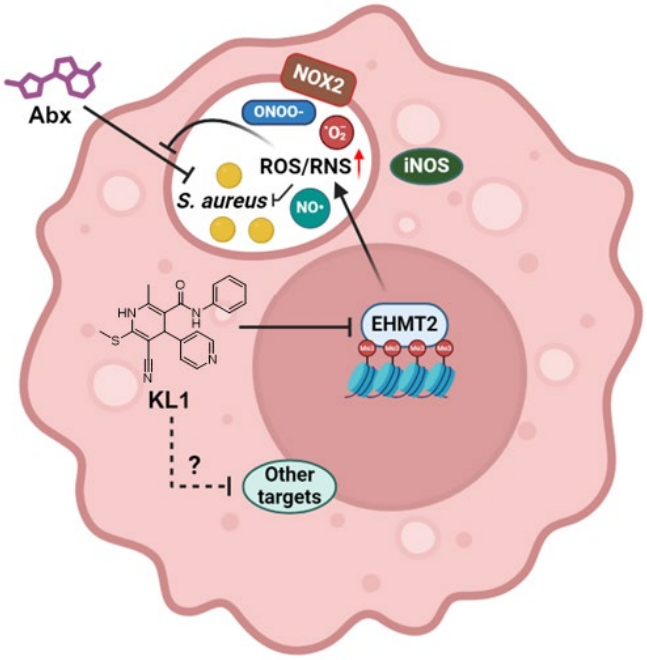

Figure 8. Mechanistic model of KL1-mediated sensitization of intracellular *S. aureus*. Host-derived reactive oxygen and nitrogen species (ROS/RNS) help contain intracellular *S. aureus* infections but also antagonize antibiotics by collapsing the bacterial metabolism and forcing the bacteria into antibiotic-tolerant persister cells. The identified compound **KL1** sensitizes intracellular bacteria to antibiotic killing by reducing the production of reactive species upon infection, presumably by targeting the G9a/EHMT2 activity.

809 **Supplementary table 1. Primers for molecular cloning.**

Primer	Sequence
mKate forward	CAAATAGGTACCTATGTCAGAACTTATCAAGGAAAATATG[†]
mKate reverse	GATTACGAATTCTTAACGGTGTC
mKate_597[‡]	CTTGTCGGTGGAGGTCAC
mKate CTC forward	CCTTGATAAGTTCTGACATAGGTACCATCctcCTTATTTTAATTATACTCTATCAATGATAG[§]
mKate GAG reverse	CTATCATTGATAGAGTATAATTAAAATAAGgagGATGGTACCTATGTCAGAACTTATCAAGG[§]

810 [†]The sequence in red represents 5' overhang containing a KpnI site.

811 [‡]Sequencing primer to confirm the identity of the gene.

812 [§]The sequence in lowercase represent inserted nucleotides for incorporating an upstream

813 ribosomal binding site.

814

815 **Supplementary table 2. Minimum inhibitory concentrations (MICs) of antibiotics in**

816 **the *S. aureus* strains used in this study.**

Antibiotics	LAC	JE2–Lux	High persister	Low persister
Rifampicin	0.008±0.004 μg/mL	0.006 μg/mL	0.006 μg/mL	0.008±0.004 μg/mL
Moxifloxacin	5 μg/mL	5 μg/mL	0.16 μg/mL	0.16 μg/mL
Vancomycin	1.33±0.58 μg/mL	1 μg/mL	1.33±0.58 μg/mL	1 μg/mL

817 Three independent experiments were conducted, and the MIC values are presented as

818 the average ± the standard deviation.

819

820

821

822

823 **Supplementary table 3. Potential targets of KL1 based on published functional**

824 **screens.**

Target	BioAssay ID†	Assay	Activity	Location, expression‡
PHOSPHO1	1565	uHTS absorbance assay for the identification of compounds that inhibit PHOSPHO1	61.5% inhibition at 13.3 μM	Intracellular, immune cells and other cell types
SLC5A7	488975	Primary cell-based screen for identification of compounds that inhibit the Choline Transporter	BScore_intRatio of -5.0281	Membrane, not detected in immune cells
SLC5A7	493221	Confirmatory screen for compounds that inhibit the Choline Transporter	50.55% inhibition at 10 μM	Membrane, not detected in immune cells
EHMT2/G9a	504332	qHTS Assay for Inhibitors of Histone Lysine Methyltransferase G9a	EC_{50} value of 25.12 μM	Intracellular, immune cells and other cell types
COPS5	651999	uHTS identification of small molecule inhibitors of Csn-mediated Deneddylation of Cullin-Ring Ligases, vis a fluorescence polarization assay	93.48% inhibition at 12.5 μM	Intracellular, immune cells and other cell types

825 †Data sourced form PubChem biological test results.

826 ‡Data sourced form Expression Atlas.

827

828

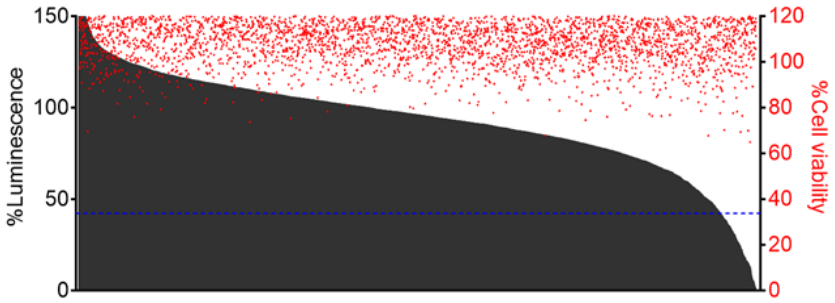

Supplementary figure 1. High-throughput screening of a kinase-targeted library identifies compounds with differential capacities in modulating the energy state of intracellular *S. aureus*. A total of >4,700 compounds (10 μM) from the UNC CICBDD were screened for targeting the intracellular MRSA. All of these compounds shared structural similarity to kinase inhibitors and complied with the Lipinski's rule of five. The luminescence signals were normalized to the vehicle controls (0.1% DMSO) (black bars). The normalized host cell viability was measured by the CellTiter-Fluor assay (red circles). The %luminescence of 10 μg/mL rifampicin-treated cells is indicated as a reference (blue dashed line).

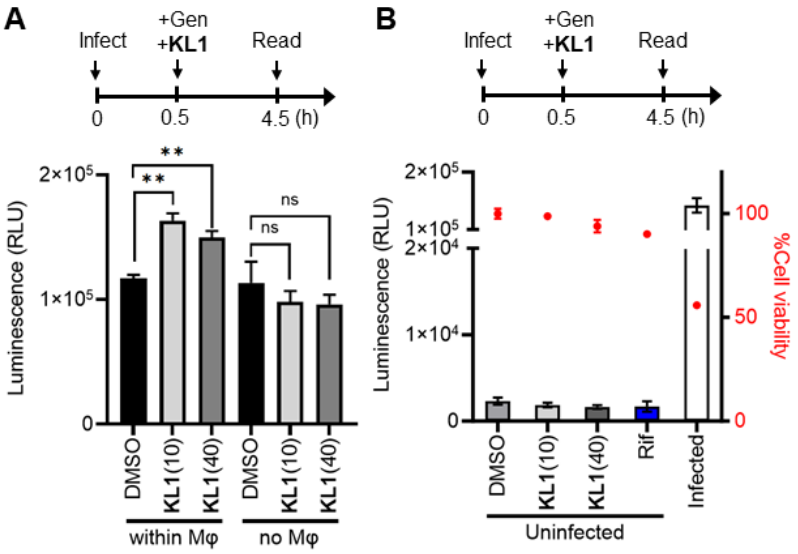

Supplementary figure 2. The energy state up-regulation by KL1 is not caused by background noise from the compound, the host cells or dead extracellular bacteria. (**A**) Macrophages infected with the bioluminescent MRSA strain JE2–lux (within Mφ) were treated with 10 μM or 40 μM **KL1**. Gentamicin (Gen; 50 μg/mL) was added to eliminate the extracellular bacteria. The bacterial cultures without macrophages (no Mφ) in the presence of Gen were examined with the same input CFU and culture conditions (n = 3). (**B**) Uninfected macrophages were treated with 10 μM or 40 μM **KL1**. The normalized host cell viability was measured by the CellTiter-Fluor assay (red circles). Rifampicin (Rif)-treated cells (blue bar) and infected macrophages (white bar) were included as controls (n = 3). Assay schematics are shown above plots. **p<0.01; ns, not significant (unpaired t-test). The bars represent mean ± SEM.

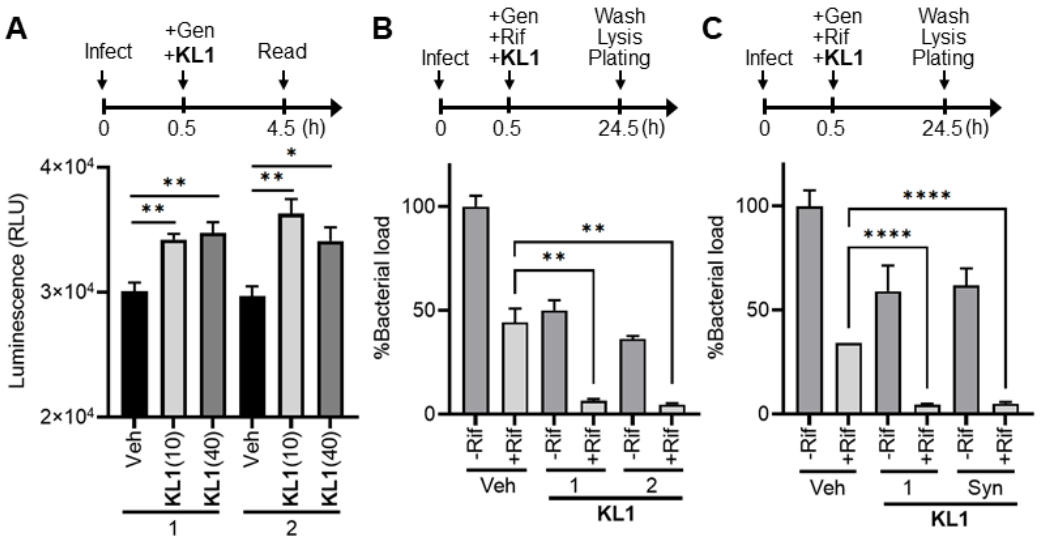

Supplementary figure 3. The adjuvant activity of KL1 was consistently observed with the compound across different sources. (**A** and **B**) **KL1** (10 and 40 μM) purchased from two independent suppliers, ChemBridge (1) and Enamine (2), consistently elevated the energy state of intracellular *S. aureus* (n = 4) and sensitized the bacteria to killing by rifampicin (Rif, 10 μg/mL) (n = 3). (**C**) **KL1** synthesized in-house (Syn) displayed adjuvant activity comparable to that of commercially available **KL1** (n = 3). Gentamicin (Gen; 50 μg/mL) was added to eradicate the extracellular bacteria. The numbers of tolerant bacteria were normalized to the untreated control (no Rif, no **KL1**, Gen-only). Assay schematics are shown above plots. *p<0.05; **p<0.01; ****p<0.0001 (unpaired t-test). The bars represent mean ± SEM.

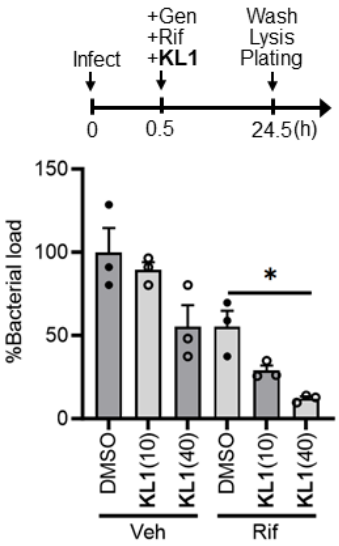

868

869 **Supplementary figure 4. Compound KL1 sensitizes the killing of intracellular MRSA**

870 **by antibiotics in a dose-dependent manner.** RAW 264.7 cells were infected with the

871 MRSA strain JE2–lux and treated with 10 μM or 40 μM **KL1** in the presence or absence

872 of 10 μg/mL rifampicin (Rif). Gentamicin (Gen; 50 μg/mL) was added to eliminate the

873 extracellular bacteria. The numbers of survivor bacteria were normalized to the untreated

874 control (no Rif, no **KL1**, Gen-only) (n = 3). *$p<0.05$ (unpaired t-test). The bars represent

875 mean ± SEM.

876

877

878

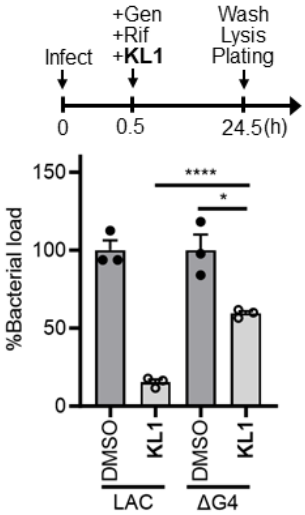

879

880 **Supplementary figure 5. Glucose uptake is important for the synergism between**
881 **KL1 and antibiotics.** RAW 264.7 cells were infected with the wild-type strain LAC or the
882 mutant lacking all four glucose transporters (ΔG4). The infected cells were treated with
883 40 μM **KL1** and 10 μg/mL rifampicin (Rif). Gentamicin (Gen) was included to eliminate
884 the extracellular bacteria. The numbers of survivor bacteria were normalized to the
885 corresponding controls (no **KL1**, Gen- and Rif-only) (black circles) (n = 3). *$p<0.05$;
886 ****$p<0.0001$ (unpaired t-test). The bars represent mean ± SEM.

887

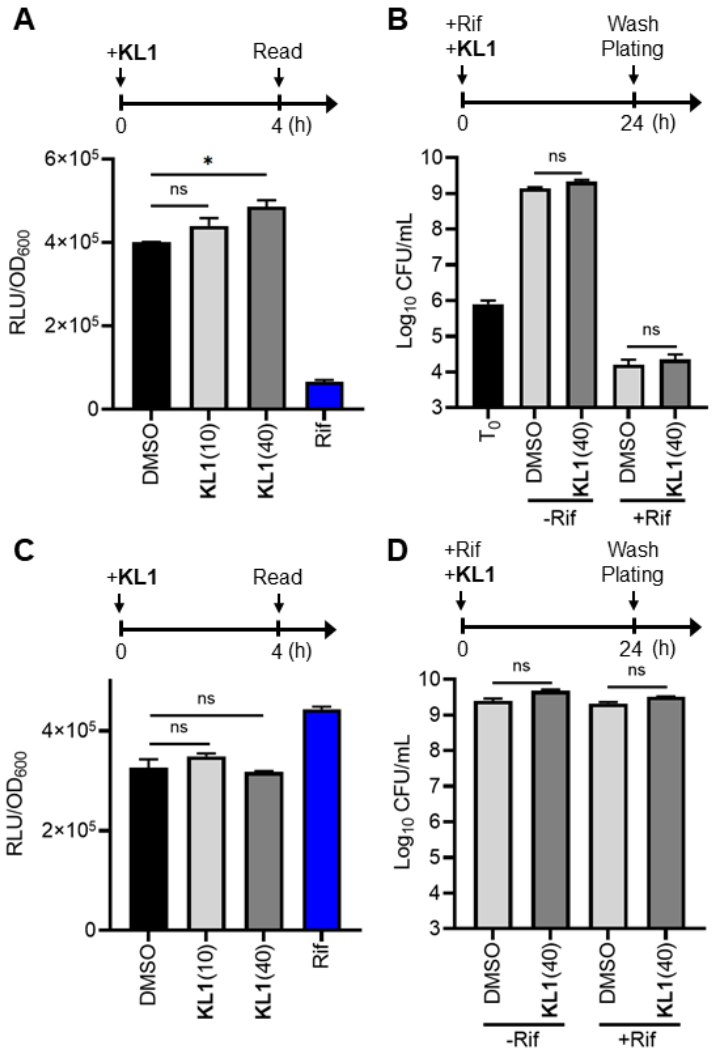

Supplementary figure 6. Compound KL1 exhibits a minute effect on the extracellular *S. aureus* activity and does not synergize with antibiotics in killing the extracellular bacteria. (**A** and **C**) The exponential-phase (**A**) and stationary-phase (**C**) *S. aureus* cultures (JE2–lux) were incubated with 10 μM or 40 μM **KL1** for 4 h, followed by luminescence detection. The signal intensities (RLU) were normalized to the OD_{600} values. The vehicle control (0.1% DMSO, black bar) and rifampicin (Rif; 2 μg/mL)-treated group (blue bar) were included as references. (**B** and **D**) The exponential-phase (**B**) and stationary-phase (**D**) cultures were treated with and without 40 μM **KL1** and 2 μg/mL Rif

897 for 24 h, followed by a wash step and plating to enumerate the number of tolerant bacteria.

898 Assay schematics are shown above plots. *$p<0.05$; ns, not significant (unpaired t-test).

899 The bars represent mean ± SEM.

900

901

902

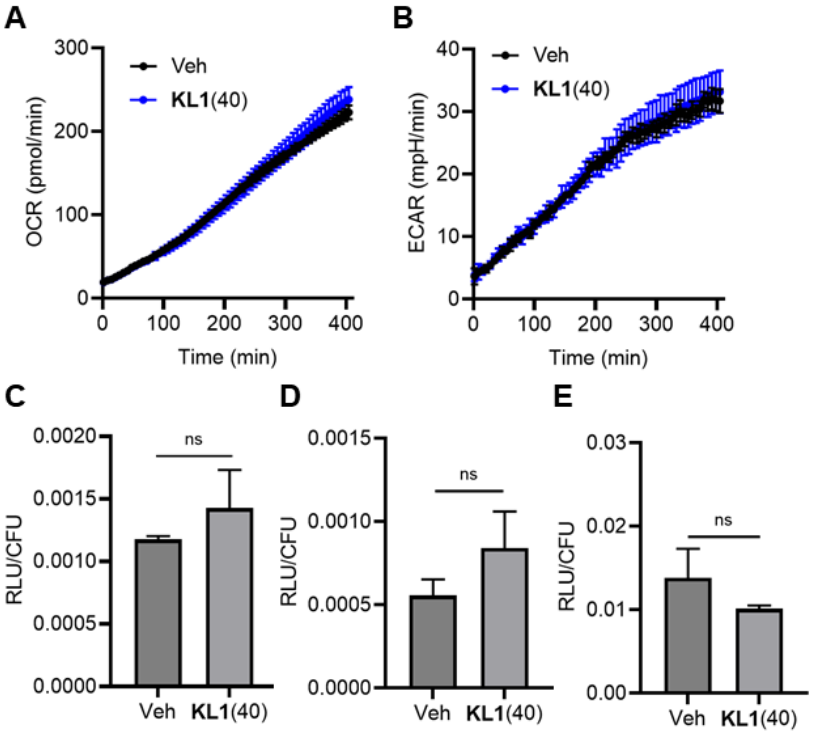

Supplementary figure 7. Compound KL1 does not impact the metabolic activity and ATP levels in extracellular bacteria. (**A** and **B**) Metabolic analysis indicates that **KL1** (40 μM, blue) does not alter the oxygen consumption rate (OCR) (**A**) and extracellular acidification rate (ECAR) (**B**) in extracellular *S. aureus* comparing to the vehicle control (Veh, 0.1–0.5% DMSO, black). Representative data of six independent experiments (n = 3) is shown. The bars represent mean ± SD. (**C**–**E**) Exponential-phase cultures were treated with 40 μM **KL1** or 0.1% DMSO for 4 h, followed by measuring the relative ATP levels using a BacTiter-Glo assay. The luminescent signals were normalized to the numbers of bacteria. *S. aureus* strains HG003 (**C**), JE2 (**D**) and LAC (**E**) were examined (n = 3–6). ns, not significant (unpaired t-test).

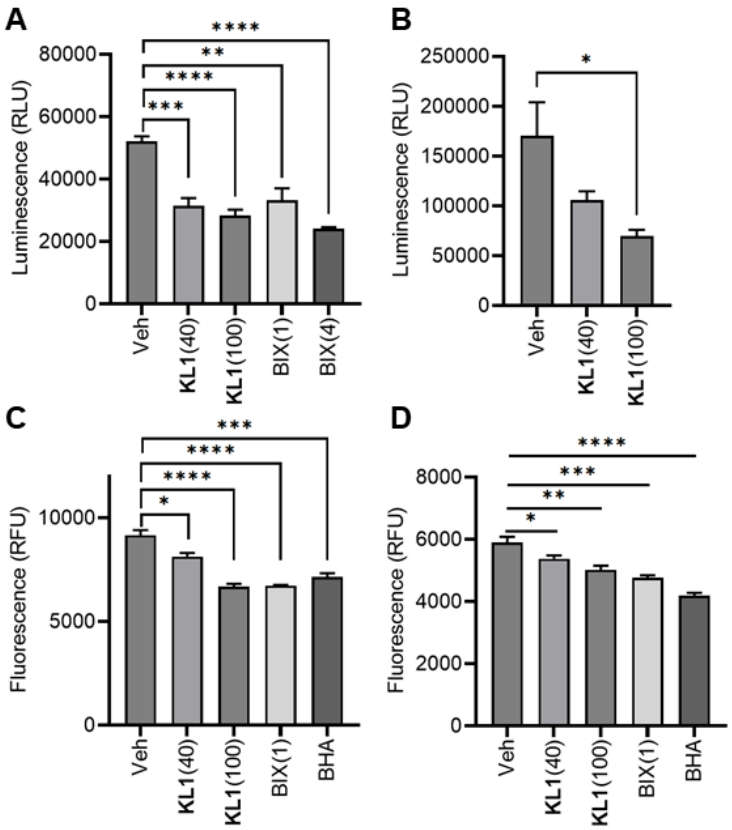

Supplementary figure 8. KL1 reduces the level of reactive species in both infected and uninfected macrophages. Compound **KL1** (40 and 100 μM) and the EHMT2/G9a inhibitor, BIX-01294 (BIX; 1 and 4 μM) decreased the ROS/RNS level in *S. aureus*-infected macrophages at 8 hours post-infection (hpi) (**A** and **C**) and in uninfected macrophages (**B** and **D**). L-012 (**A** and **B**) and fluorescein-boronate (Fl-B) (**C** and **D**) were used to quantify the ROS/RNS level. DMSO (Veh; 0.25%) and butylated hydroxyanisole (BHA; 20 μM) were included as controls. Representative data of three independent experiments are shown (n = 5). *p<0.05; **p<0.01; ***p<0.001; ****p<0.0001 (unpaired t-test). The bars represent mean ± SEM.

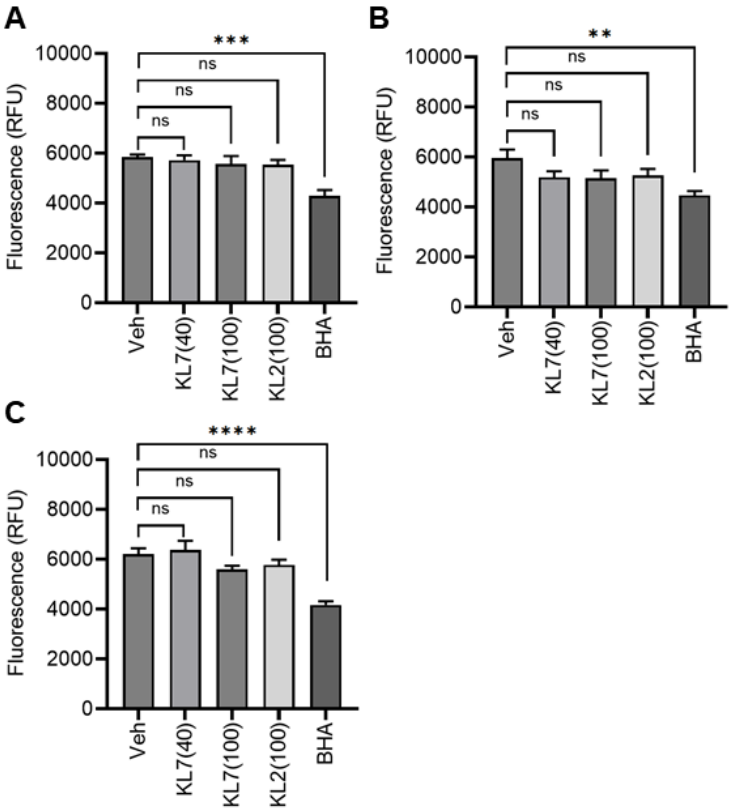

929

930 **Supplementary figure 9. The inactive analog of KL1 losses the ability to reduce the**
931 **level of reactive species in both infected and uninfected macrophages.** The inactive
932 analog KL7 (40 and 100 μM) and analog KL2 (100 μM) with lower adjuvant activity did
933 not affect ROS/RNS production in uninfected (**A** and **B**) and *S. aureus*-infected
934 macrophages (**C**) after 4 h (**A**) and 8 h (**B** and **C**) treatment. Fluorescein-boronate (Fl-B)
935 was used to quantify the level of reactive species. DMSO (Veh; 0.25%) and butylated
936 hydroxyanisole (BHA; 20 μM) were included as controls. Representative data of three
937 independent experiments are shown (n = 5). **p<0.01; ***p<0.001; ****p<0.0001; ns, not
938 significant (unpaired t-test). The bars represent mean ± SEM.

939

940 ## References

941 1. M. Huemer *et al.*, Molecular reprogramming and phenotype switching in
942 Staphylococcus aureus lead to high antibiotic persistence and affect therapy
943 success. *Proc Natl Acad Sci U S A* **118** (2021).
944 2. N. D. Hicks *et al.*, Clinically prevalent mutations in Mycobacterium tuberculosis
945 alter propionate metabolism and mediate multidrug tolerance. *Nat Microbiol* **3**,
946 1032-1042 (2018).
947 3. R. A. Fisher, B. Gollan, S. Helaine, Persistent bacterial infections and persister
948 cells. *Nat Rev Microbiol* **15**, 453-464 (2017).
949 4. L. F. Westblade, J. Errington, T. Dorr, Antibiotic tolerance. *PLoS Pathog* **16**,
950 e1008892 (2020).
951 5. N. Q. Balaban *et al.*, Definitions and guidelines for research on antibiotic
952 persistence. *Nat Rev Microbiol* **17**, 441-448 (2019).
953 6. K. Y. Lu *et al.*, Antibiotic Tolerance and Treatment Outcomes in Cystic Fibrosis
954 Methicillin-Resistant Staphylococcus aureus Infections. *Microbiol Spectr* **11**,
955 e0406122 (2023).
956 7. R. Kuehl, L. Morata, S. Meylan, J. Mensa, A. Soriano, When antibiotics fail: a
957 clinical and microbiological perspective on antibiotic tolerance and persistence of
958 Staphylococcus aureus. *J Antimicrob Chemother* **75**, 1071-1086 (2020).
959 8. I. Levin-Reisman *et al.*, Antibiotic tolerance facilitates the evolution of resistance.
960 *Science* **355**, 826-830 (2017).
961 9. I. Santi, P. Manfredi, E. Maffei, A. Egli, U. Jenal, Evolution of Antibiotic Tolerance
962 Shapes Resistance Development in Chronic Pseudomonas aeruginosa Infections.
963 *mBio* **12** (2021).

964 10. B. P. Conlon *et al.*, Persister formation in Staphylococcus aureus is associated with
965 ATP depletion. *Nat Microbiol* **1** (2016).
966 11. M. L. Pinel-Marie *et al.*, RNA antitoxin SprF1 binds ribosomes to attenuate
967 translation and promote persister cell formation in Staphylococcus aureus. *Nat*
968 *Microbiol* **6**, 209-220 (2021).
969 12. J. A. Freiberg *et al.*, Restriction of arginine induces antibiotic tolerance in
970 Staphylococcus aureus. *Nat Commun* **15**, 6734 (2024).
971 13. B. W. Kwan, J. A. Valenta, M. J. Benedik, T. K. Wood, Arrested protein synthesis
972 increases persister-like cell formation. *Antimicrob Agents Chemother* **57**, 1468-
973 1473 (2013).
974 14. S. Song, T. K. Wood, Persister cells resuscitate via ribosome modification by 23S
975 rRNA pseudouridine synthase RluD. *Environ Microbiol* **22**, 850-857 (2020).
976 15. S. E. Rowe *et al.*, Reactive oxygen species induce antibiotic tolerance during
977 systemic Staphylococcus aureus infection. *Nat Microbiol* **5**, 282-290 (2020).
978 16. J. E. Beam *et al.*, Macrophage-Produced Peroxynitrite Induces Antibiotic Tolerance
979 and Supersedes Intrinsic Mechanisms of Persister Formation. *Infect Immun* **89**,
980 e0028621 (2021).
981 17. F. Peyrusson *et al.*, Intracellular Staphylococcus aureus persisters upon antibiotic
982 exposure. *Nat Commun* **11**, 2200 (2020).
983 18. S. Helaine *et al.*, Internalization of Salmonella by macrophages induces formation
984 of nonreplicating persisters. *Science* **343**, 204-208 (2014).
985 19. Y. Liu *et al.*, Immune activation of the host cell induces drug tolerance in
986 Mycobacterium tuberculosis both in vitro and in vivo. *J Exp Med* **213**, 809-825
987 (2016).

988 20. S. Helaine, B. P. Conlon, K. M. Davis, D. G. Russell, Host stress drives tolerance
989 and persistence: The bane of anti-microbial therapeutics. *Cell Host Microbe* **32**,
990 852-862 (2024).
991 21. F. Peyrusson, T. K. Nguyen, T. Najdovski, F. Van Bambeke, Host Cell Oxidative
992 Stress Induces Dormant Staphylococcus aureus Persisters. *Microbiol Spectr* **10**,
993 e0231321 (2022).
994 22. J. R. Raneses, A. L. Ellison, B. Liu, K. M. Davis, Subpopulations of Stressed
995 Yersinia pseudotuberculosis Preferentially Survive Doxycycline Treatment within
996 Host Tissues. *mBio* **11** (2020).
997 23. P. W. S. Hill *et al.*, The vulnerable versatility of Salmonella antibiotic persisters
998 during infection. *Cell Host Microbe* **29**, 1757-1773 e1710 (2021).
999 24. S. H. Hong, X. Wang, H. F. O'Connor, M. J. Benedik, T. K. Wood, Bacterial
1000 persistence increases as environmental fitness decreases. *Microb Biotechnol* **5**,
1001 509-522 (2012).
1002 25. B. G. Surewaard *et al.*, Identification and treatment of the Staphylococcus aureus
1003 reservoir in vivo. *J Exp Med* **213**, 1141-1151 (2016).
1004 26. P. Sendi, R. A. Proctor, Staphylococcus aureus as an intracellular pathogen: the
1005 role of small colony variants. *Trends Microbiol* **17**, 54-58 (2009).
1006 27. S. Clement *et al.*, Evidence of an intracellular reservoir in the nasal mucosa of
1007 patients with recurrent Staphylococcus aureus rhinosinusitis. *J Infect Dis* **192**,
1008 1023-1028 (2005).
1009 28. R. S. Flannagan, B. Heit, D. E. Heinrichs, Intracellular replication of
1010 Staphylococcus aureus in mature phagolysosomes in macrophages precedes host
1011 cell death, and bacterial escape and dissemination. *Cell Microbiol* **18**, 514-535

1012 (2016).
1013 29. C. Garzoni, W. L. Kelley, Staphylococcus aureus: new evidence for intracellular
1014 persistence. *Trends Microbiol* **17**, 59-65 (2009).
1015 30. P. Nandhini *et al.*, Recent Developments in Methicillin-Resistant Staphylococcus
1016 aureus (MRSA) Treatment: A Review. *Antibiotics (Basel)* **11** (2022).
1017 31. P. Santucci *et al.*, Intracellular localisation of Mycobacterium tuberculosis affects
1018 efficacy of the antibiotic pyrazinamide. *Nat Commun* **12**, 3816 (2021).
1019 32. S. Ronneau, C. Michaux, R. T. Giorgio, S. Helaine, Intoxication of antibiotic
1020 persisters by host RNS inactivates their efflux machinery during infection. *PLoS*
1021 *Pathog* **20**, e1012033 (2024).
1022 33. P. Hovhannisyan *et al.*, Infection of human organoids supports an intestinal niche
1023 for Chlamydia trachomatis. *PLoS Pathog* **20**, e1012144 (2024).
1024 34. H. Liu *et al.*, Staphylococcus aureus Epicutaneous Exposure Drives Skin
1025 Inflammation via IL-36-Mediated T Cell Responses. *Cell Host Microbe* **22**, 653-666
1026 e655 (2017).
1027 35. L. R. Thurlow, A. C. Stephens, K. E. Hurley, A. R. Richardson, Lack of nutritional
1028 immunity in diabetic skin infections promotes Staphylococcus aureus virulence.
1029 *Sci Adv* **6** (2020).
1030 36. M. A. Lobritz *et al.*, Antibiotic efficacy is linked to bacterial cellular respiration. *Proc*
1031 *Natl Acad Sci U S A* **112**, 8173-8180 (2015).
1032 37. C. UniProt, UniProt: the Universal Protein Knowledgebase in 2023. *Nucleic Acids*
1033 *Res* **51**, D523-D531 (2023).
1034 38. E. W. Sayers *et al.*, Database resources of the national center for biotechnology
1035 information. *Nucleic Acids Res* **50**, D20-D26 (2022).

1036 39. K. L. Cotten, K. M. Davis, Bacterial heterogeneity and antibiotic persistence:
1037 bacterial mechanisms utilized in the host environment. *Microbiol Mol Biol Rev* **87**,
1038 e0017422 (2023).
1039 40. Y. Li, G. Li, L. Zhang, Y. Li, Z. Zhao, G9a promotes inflammation in Streptococcus
1040 pneumoniae induced pneumonia mice by stimulating M1 macrophage polarization
1041 and H3K9me2 methylation in FOXP1 promoter region. *Ann Transl Med* **10**, 583
1042 (2022).
1043 41. A. Muneer *et al.*, Non-canonical function of histone methyltransferase G9a in the
1044 translational regulation of chronic inflammation. *Cell Chem Biol* **30**, 1525-1541
1045 e1527 (2023).
1046 42. X. Wang *et al.*, Histone methyltransferases G9a mediated lipid-induced M1
1047 macrophage polarization through negatively regulating CD36. *Metabolism* **114**,
1048 154404 (2021).
1049 43. S. Scheer, C. Zaph, The Lysine Methyltransferase G9a in Immune Cell
1050 Differentiation and Function. *Front Immunol* **8**, 429 (2017).
1051 44. C. Liu *et al.*, A chromatin activity-based chemoproteomic approach reveals a
1052 transcriptional repressome for gene-specific silencing. *Nat Commun* **5**, 5733
1053 (2014).
1054 45. N. Rios *et al.*, Sensitive detection and estimation of cell-derived peroxynitrite fluxes
1055 using fluorescein-boronate. *Free Radic Biol Med* **101**, 284-295 (2016).
1056 46. C. Liu *et al.*, Clinical practice guidelines by the infectious diseases society of
1057 america for the treatment of methicillin-resistant Staphylococcus aureus infections
1058 in adults and children. *Clin Infect Dis* **52**, e18-55 (2011).
1059 47. A. D. Bai *et al.*, Staphylococcus aureus bacteraemia mortality: a systematic review

1060 and meta-analysis. *Clin Microbiol Infect* **28**, 1076-1084 (2022).
1061 48. J. Tasse, G. Dieppois, F. Peyrane, N. Tesse, Improving the ability of antimicrobial
1062 susceptibility tests to predict clinical outcome accurately: Adding metabolic evasion
1063 to the equation. *Drug Discov Today* **26**, 2182-2189 (2021).
1064 49. H. Niu, J. Gu, Y. Zhang, Bacterial persisters: molecular mechanisms and
1065 therapeutic development. *Signal Transduct Target Ther* **9**, 174 (2024).
1066 50. B. Gollan, G. Grabe, C. Michaux, S. Helaine, Bacterial Persisters and Infection:
1067 Past, Present, and Progressing. *Annu Rev Microbiol* **73**, 359-385 (2019).
1068 51. A. Harms, E. Maisonneuve, K. Gerdes, Mechanisms of bacterial persistence
1069 during stress and antibiotic exposure. *Science* **354** (2016).
1070 52. D. D. Rockey, X. Wang, A. Debrine, N. Grieshaber, S. S. Grieshaber, Metabolic
1071 dormancy in Chlamydia trachomatis treated with different antibiotics. *Infect Immun*
1072 **92**, e0033923 (2024).
1073 53. I. Keren, S. Minami, E. Rubin, K. Lewis, Characterization and transcriptome
1074 analysis of Mycobacterium tuberculosis persisters. *mBio* **2**, e00100-00111 (2011).
1075 54. C. H. Luk *et al.*, Salmonella enters a dormant state within human epithelial cells
1076 for persistent infection. *PLoS Pathog* **17**, e1009550 (2021).
1077 55. W. Eisenreich, T. Rudel, J. Heesemann, W. Goebel, Persistence of Intracellular
1078 Bacterial Pathogens-With a Focus on the Metabolic Perspective. *Front Cell Infect*
1079 *Microbiol* **10**, 615450 (2020).
1080 56. J. E. Beam *et al.*, Inflammasome-mediated glucose limitation induces antibiotic
1081 tolerance in Staphylococcus aureus. *iScience* **26**, 107942 (2023).
1082 57. E. Blasi *et al.*, Selective immortalization of murine macrophages from fresh bone
1083 marrow by a raf/myc recombinant murine retrovirus. *Nature* **318**, 667-670 (1985).

1084 58. B. T. Bateman, N. P. Donegan, T. M. Jarry, M. Palma, A. L. Cheung, Evaluation of
1085 a tetracycline-inducible promoter in Staphylococcus aureus in vitro and in vivo and
1086 its application in demonstrating the role of sigB in microcolony formation. *Infect*
1087 *Immun* **69**, 7851-7857 (2001).
1088 59. M. R. Grosser, A. R. Richardson, Method for Preparation and Electroporation of S.
1089 aureus and S. epidermidis. *Methods Mol Biol* **1373**, 51-57 (2016).
1090 60. N. W. de Jong, T. van der Horst, J. A. van Strijp, R. Nijland, Fluorescent reporters
1091 for markerless genomic integration in Staphylococcus aureus. *Sci Rep* **7**, 43889
1092 (2017).
1093 61. R. M. Corrigan, T. J. Foster, An improved tetracycline-inducible expression vector
1094 for Staphylococcus aureus. *Plasmid* **61**, 126-129 (2009).
1095 62. J. Schindelin *et al.*, Fiji: an open-source platform for biological-image analysis. *Nat*
1096 *Methods* **9**, 676-682 (2012).
1097 63. R. Nistala, A. Meuth, C. Smith, A. Annayya, Reliable and High Efficiency Extraction
1098 of Kidney Immune Cells. *J Vis Exp* 10.3791/54368 (2016).
1099 64. S. Kim *et al.*, PubChem 2023 update. *Nucleic Acids Res* **51**, D1373-D1380 (2023).
1100 65. I. Papatheodorou *et al.*, Expression Atlas: gene and protein expression across
1101 multiple studies and organisms. *Nucleic Acids Res* **46**, D246-D251 (2018).
1102 66. D. Szklarczyk *et al.*, The STRING database in 2023: protein-protein association
1103 networks and functional enrichment analyses for any sequenced genome of
1104 interest. *Nucleic Acids Res* **51**, D638-D646 (2023).
1105